TWO-PHASE FLOW IN AN INCLINED PIPE

By

DOMINGO L. MORENO BELTRÁN

Ingeniero Industrial

Superior Technical School of

Industrial Engineering

Madrid, Spain

1970

Submitted to the Faculty of the Graduate College
of the Oklahoma State University
in partial fulfillment of the requirements
for the Degree of
MASTER OF SCIENCE
July, 1972

TWO-PHASE FLOW IN AN INCLINED PIPE

Thesis Approved:

Thesis Adviser

Dean of the Graduate College

ACKNOWLEDGMENTS

I have received assistance from a number of people during the course of this project: I am indebted to Dr Kenneth J. Bell, my adviser, for his aid and suggestions in relation to my study in graduate school as well as to my thesis; I also want to express my thanks to Dr. John B. West for securing for me part of the equipment, and to Mr. Gene E. McCroskey for his help in the construction of the apparatus. I wish to express gratitude to Mr. Larry Hazelwood who processed and printed the photographs.

I am also indebted to Oklahoma State University, which provided me with the experimental laboratory facilities and especially to the Ministry of Education and Science of Spain, which provided me with a scholarship for this project.

TABLE OF CONTENTS

LIST OF TABLES

LIST OF FIGURES

CHAPTER I

INTRODUCTION

Knowledge of two-phase flow has been limited primarily to horizontal and vertical upward flow and very little is known about two-phase flow in inclined pipes. The nomenclature for the various visually observed types of flow is in a state of confusion, as each investigator uses slightly different terms. It would be desirable to develop general theories to explain the experimental observations so that a more objective method to characterize the flow patterns could be found.

The pressure drop in two-phase flow is much higher than in single-phase flow. Experimental data confirm the fact that the pressure drop for a two-phase flow system is influenced by the flow pattern. Therefore, it is necessary to incorporate into pressure drop calculations those variables which in fact define the flow pattern so we can predict both the flow pattern and the pressure drop.

Two-phase flow is a problem of great importance in condensation and boiling heat transfer, in nuclear engineering, oil and gas production and transportation equipment, and cryogenic processes. Thus, it is vital to know the fluid dynamics and the flow regimes involved to be able to choose the proper correlation to predict the heat transfer coefficient at each point.

The following goals were set for this project:

1. Design, construct and operate an apparatus to study two-phase

flow patterns in horizontal pipes and those inclined at 5° and 15°, based upon visual observations of air-water flow mixtures.

2. Take photographs of the characteristic flow regimes to help interpret the visual observations and conclusions obtained.

3. Make pressure drop measurements.

4. Correlate the data in an attempt to learn how the flow patterns and pressure drop change as the angle of inclination and the flow rates of air and water are changed.

The types of two-phase flow patterns depend upon the relative and absolute quantities of the fluids, the physical properties of the fluids, the geometric configuration of the conduit, and occasionally upon the heat transfer process. In general, we can say that gravity and vapor shear forces acting in different directions determine the flow regime. For small diameter conduits and low flow rates, surface tension forces should also be considered.

This study will consider the seven typical flow regimes according to Alves' nomenclature (1). Further, these flow regimes will be defined according to the visual observations made, bearing in mind that the experiment was conducted in isothermal and adiabatic conditions with both fluids, air and water, at near room temperature. Flow pattern sketches are shown in Figure 1. Photographs of the typical flow regimes with indications of the transformed Baker's map coordinates are shown in Appendix B. The seven typical flow regimes are as follows:

1. Bubble flow: Bubbles of gas are dispersed throughout the liquid. In the experiment bubbles were found only at the top of the pipe.

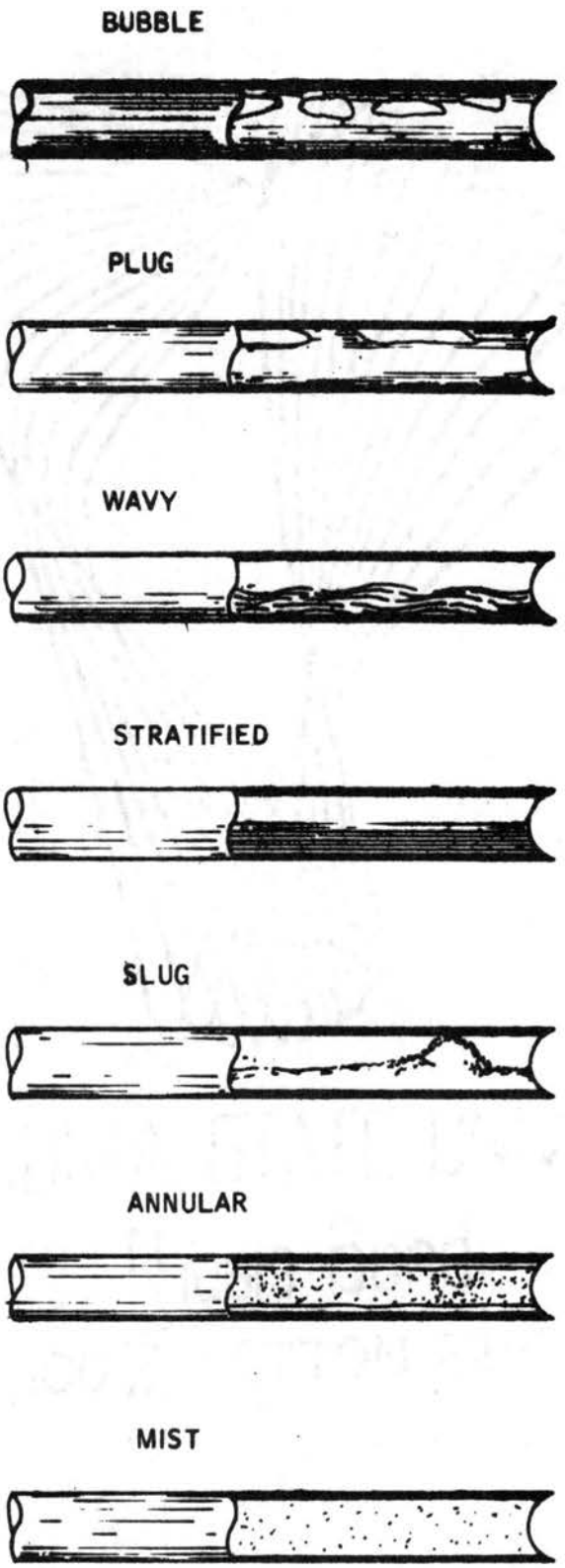

Figure 1. Flow Pattern Sketches

However, it has been observed by other researchers, and it is logical, that at higher air flow rates those bubbles will be dispersed throughout the cross-section.

2. Plug flow: Alternate plugs of liquid and gas move along the upper part of the pipe. Sometimes the plugs decrease in size as they travel and this could be interpreted as a tendency to change the flow regime. In fact, when the pipe is inclined, plug flow at the inlet becomes bubble flow at the outlet. Closer to the slug zone, the plugs become larger and the pressure drop oscillates more.

3. Stratified flow: The liquid flows along the bottom of the pipe and the gas flows over a smooth liquid-gas interface. Over most of the stratified region, however, the mixing tee and external effects superimposed waves and slugs on the stratified flow making it difficult to define the transition line to other flow regimes.

4. Wavy flow: The gas moves at a higher velocity than the liquid producing a rough gas-liquid interface with waves traveling in the direction of flow; still the liquid flows along the bottom of the pipe.

The transition from wavy to annular is difficult to distinguish because it occurs gradually. The waves travel faster and the water climbs the wall of the pipe although it is thicker at the bottom of the pipe. An axial view will show a core of gas forming.

5. Slug flow: A wave is picked up periodically by the rapidly moving gas to form a frothy slug which passes along the pipe at a greater velocity than the average liquid velocity. The slugs accelerate as they move through the pipe. These waves of liquid completely fill the pipe at a given cross section, while at other points the pipe cross section is filled with both air and water. These slugs cause large pulsa-

tions in the pressure drop readings because of the impact of the high velocity waves in bends and fittings of the pipe.

The transition from slug to annular flow occurs when the slugs begin to travel so fast that it is impossible for the human eye to distinguish one from the other, although a high speed camera could be used to follow these fast slugs.

6. Annular flow: All the liquid flows as a film annulus around the pipe inner wall and the gas flows as a core with a small portion of the liquid entrained by the central gas core.

The transition from annular flow to mist seems to occur when the high air flow rates disperse some of the liquid film into the gas core.

7. Mist flow: Most of the liquid is carried as fine drops by the gas phase; that is to say, most of the liquid is entrained as fine droplets by the gas while a small portion of the liquid flows as an annulus on the pipe wall.

CHAPTER II

LITERATURE REVIEW

Flow Pattern Maps in Horizontal Pipe

Alves (1) defined the flow patterns that most of the investigators have used.

Baker (2) employed the flow pattern definitions set forth by Alves, adopted the data of Gazley, Jenkins, Alves and Kosterin, and presented a generalized plot of the flow pattern regions as shown in Figure 2.

Baker observed that, although the borders of the various flow pattern regions are shown as lines, in reality these borders are rather broad transition zones. Since most of the available data were for the air-water system at atmospheric pressure, correction factors suggested by Holmes were introduced to adjust for other liquids and gases.

$$\lambda = \left[\left(d_v/0.075\right)\left(d_\ell/62.3\right)\right]^{\frac{1}{2}} \tag{2.1}$$

$$\overline{\psi} = \left(73/\sigma\right)\left[\mu_\ell\left(62.3/d_\ell\right)^2\right]^{\frac{1}{3}} \tag{2.2}$$

There have been many modifications to this flow pattern map, such as those made by Scott (3) and Newson (3). They use the same nomenclature but show different transition lines.

White and Huntington (4) proposed some variations on Alves' definitions of flow patterns and also presented their results of flow pattern

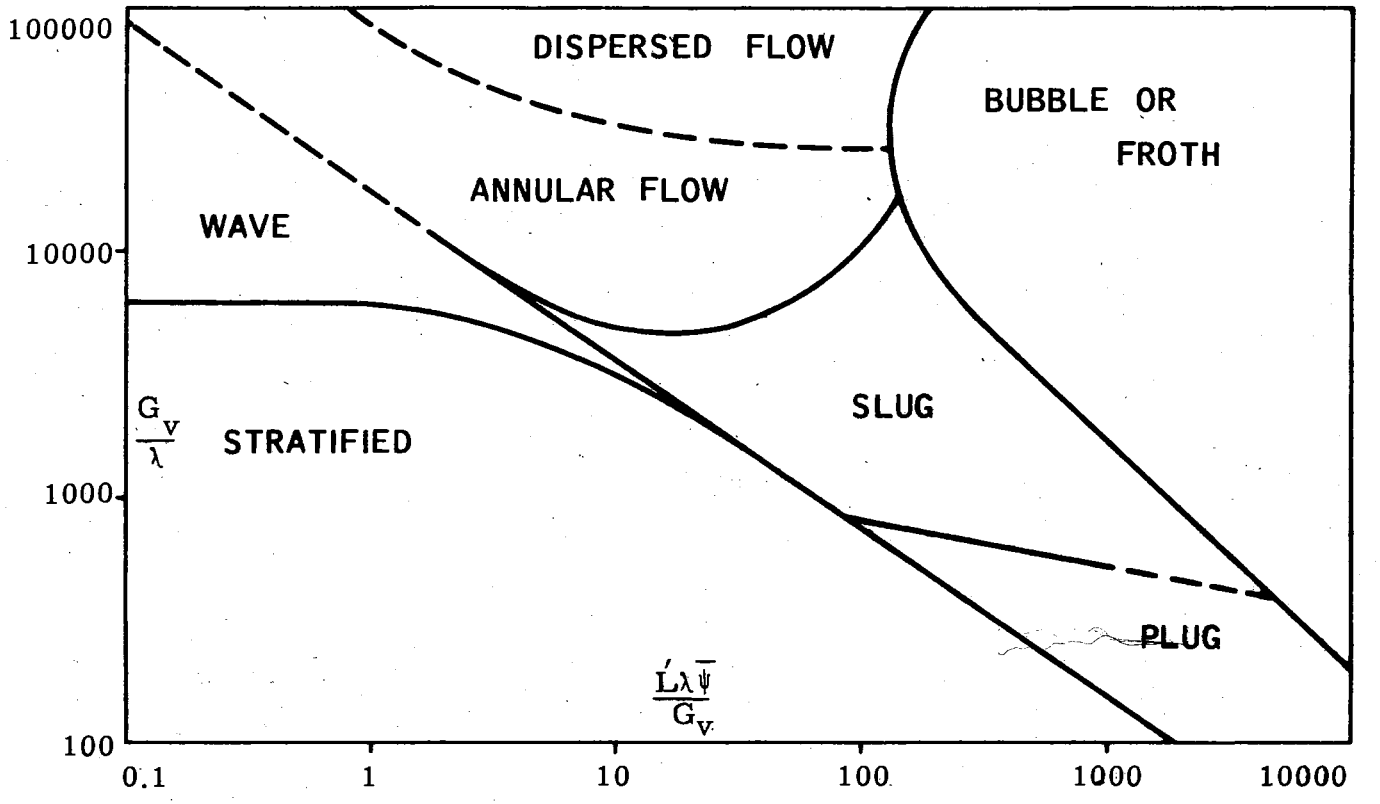

Figure 2. Original Baker's Flow Pattern Regions

studies in terms of gas and liquid flow rates with noticeable differences from the Baker map.

Govier (5) too presents his results in terms of mass velocity of air and water showing noticeable differences from the Baker map also, though not as great as those shown by White and Huntington.

Schicht (6) uses a superficial mass velocity of air as ordinate and a dimensionless parameter, $M_\ell^* \lambda \psi / M_G^*$, in the x-axis. His results show the general form of the Baker map with some differences.

Hoogendoorn (7) follows Kosterin in the presentation of his results. He uses a gas flow weight quality of mixture and a superficial mixture velocity, obtaining a general diagram for flow regions of completely different shapes than Baker and therefore difficult to compare.

Alves (1) presents his results in terms of the liquid and gas superficial velocities; Krasiakova (8) also uses liquid and gas superficial velocities. Neither of them found all seven flow patterns in their results and again obtained a map completely different from that of Baker.

Gazley (9) and Abou-Sabe (10) have presented maps in terms of air and water mass flow rates, but both lack some of the flow regimes.

Richardson (11) presented flow pattern boundaries (transition lines) in channels, expressing his results in terms of air and water mass flow rates.

Quandt's Flow Pattern Classification

Quandt (12) considers that the phase configurations are determined by a dominant force in each region. A change in the dominant force is reflected as a change in the observed flow pattern as it adjusts to the new circumstances. The assumptions are:

1. Gas and liquid flow in the same direction in a closed duct.

2. Flow field is fully developed and uniform over the duct length.

3. Frictional effects act primarily in the neighborhood of the duct walls.

The forces acting on a fluid element are those due to the axial pressure gradient, the gravitational attraction, and the interfacial surface tension. The criteria are:

a. $|\text{gravity force}| < |\text{pressure gradient force}|$

$$\bar{F}_r = \frac{\bar{v}^2}{g D_e} > \frac{2}{f_{TP}} \left(\frac{d_\ell}{\bar{d}} - \cos \alpha \right) \tag{2.3}$$

b. $|\text{axial pressure gradient}| > |\text{surface tension forces}|$

$$\bar{W}_e = \frac{\bar{v}^2 \bar{d} D_e}{\sigma g_c} > \frac{2}{f_{TP}} \left(16 - \frac{\bar{W}_e}{\bar{F}_r} \log \alpha \right) \tag{2.4}$$

c. $|\text{gravity force}| > |\text{surface tension forces}|$

$$\left(\frac{d_\ell}{\bar{d}} \right) \frac{\bar{W}_e}{\bar{F}_r} = \frac{d_\ell D_e^2 g}{\sigma g_c} > 16 \tag{2.5}$$

For slug,

$$\bar{F}_r = \frac{\bar{v}^2}{g D_e} < \frac{2}{f} \tag{2.6}$$

Quandt has compared Equations (2.3) and (2.6) with the lines shown on the Baker map finding good agreement. He proposes a classification of gas liquid flow patterns as indicated in Figure 3.

Flow Pattern Maps in Vertical Pipe

For vertical flow, Govier (13) points out the following definitions of flow patterns:

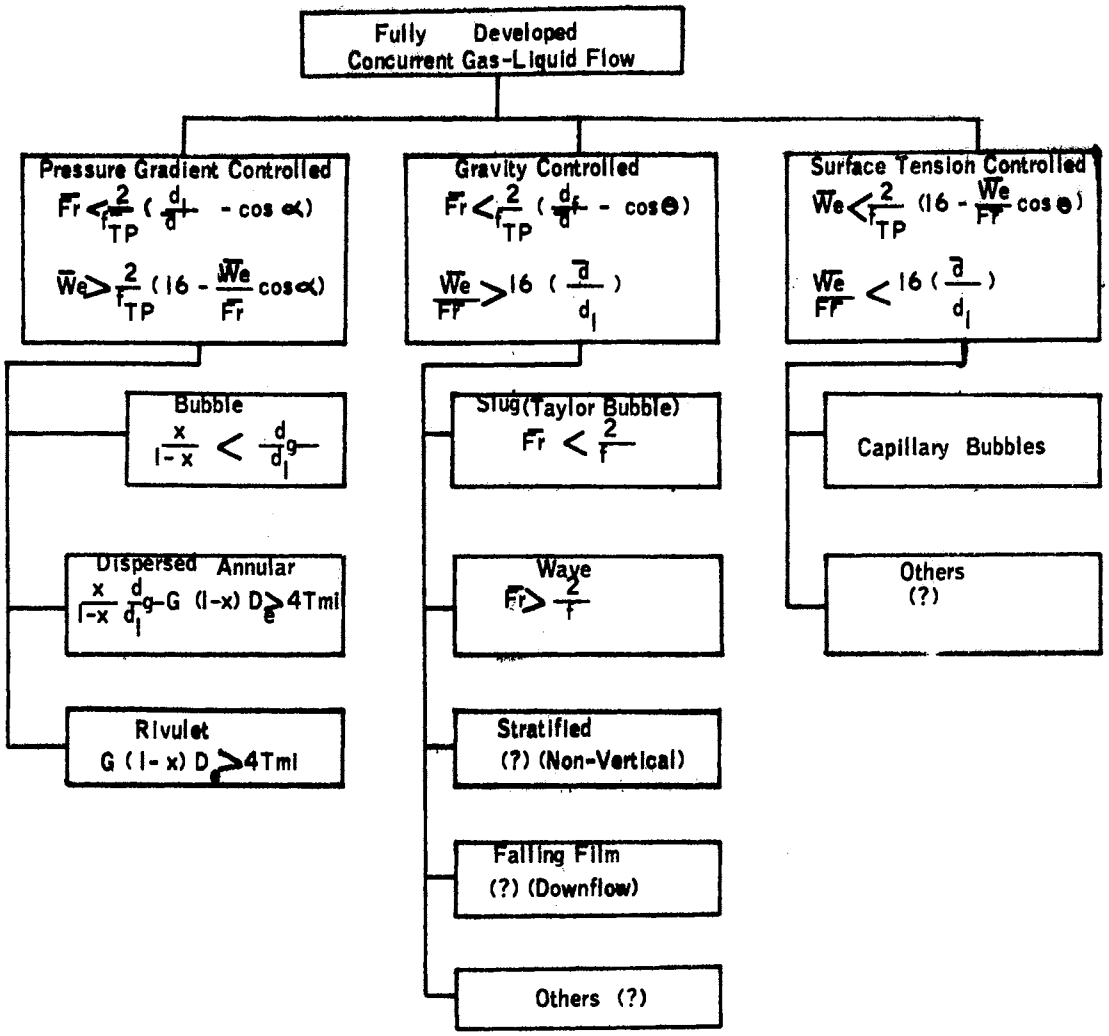

Figure 3. Quandt's Flow Pattern Classification

(a) Bubble flow: The upward flowing liquid forms the continuous phase with the gas dispersed in individual bubbles, which increase in size, number and velocity as the gas flow increases.

(b) Slug flow: The gas flows as large bullet shaped bubbles, which alternate with slugs of liquid frequently containing small gas bubbles. As the gas rate increases, the length, and upward velocity of the large bubbles increase. Each bubble is surrounded by a thin annulus of less rapidly moving liquid which flows into the underlying more rapidly moving liquid slug.

(c) Froth: In froth flow, the tendency of the liquid to fall downward past the bubbles diminishes and the bubbles degenerate merging with the liquid into a highly turbulent, patternless mixture.

(d) Annular flow: This type of flow is characterized by gas, with more or less liquid entrained as droplets, flowing upward in the central part of the tube and with the remainder of the liquid travelling upward, but more slowly, as an annular film on the walls of the tube.

(e) Mist: At higher gas velocities than exist in annular flow, droplets of liquid are captured from the film by the gas core until the mixture moves up the tube as a mist.

Kozlov (14) defined the flow pattern boundaries in terms of the discharge gas volume fraction and a discharge-mixture Froude number. Galegar, Stovall and Huntington (15) presented empirical correlations in terms of mass velocities. Govier (13) presented empirical correlations in terms of superficial water velocity and a dimensional product involving air-water volume ratio, air density and pipe diameter. Griffith and Wallis (16) followed Kozlov's nomenclature. Ros (17)

defined the flow pattern boundaries in terms of dimensionless gas and liquid velocity numbers.

The two-phase vertical flow maps presented by Golan and Stenning (18) are probably among the most representative ones and are shown in Figures 4 and 5.

A typical flow regime map developed with electrical probe (19) is shown in Figure 6.

Pressure Drop

Pressure drop in two-phase flow is more complex than in a single-phase flow.

The experimentally measured pressure drop, $(\Delta P/\Delta L)_M$, represents the combined effects of friction, acceleration and elevation changes in the direction of flow.

A simplified form of the mechanical energy equation applied to a two-phase flow is:

$$\left(\frac{\Delta P}{\Delta L}\right)_M = \left(\frac{\Delta P}{\Delta L}\right)_f + \frac{G_v^2}{g_c \Delta L}\left[\frac{1}{[d_v R_v]_2} - \frac{1}{[d_v R_v]_1}\right]$$

$$+ \frac{G_L^2}{g_c \Delta L}\left[\frac{1}{[d_\ell(1-R_v)]_2} - \frac{1}{[d_\ell(1-R_v)]_1}\right]$$

$$+ \frac{g}{g_c \Delta L}\int_{h_1}^{h_2}\left[d_\ell(1-R_v) + d_v R_v\right]dh \qquad (2.7)$$

where R_v is the void fraction, the actual volume occupied by the vapor phase divided by the total volume of the conduit,

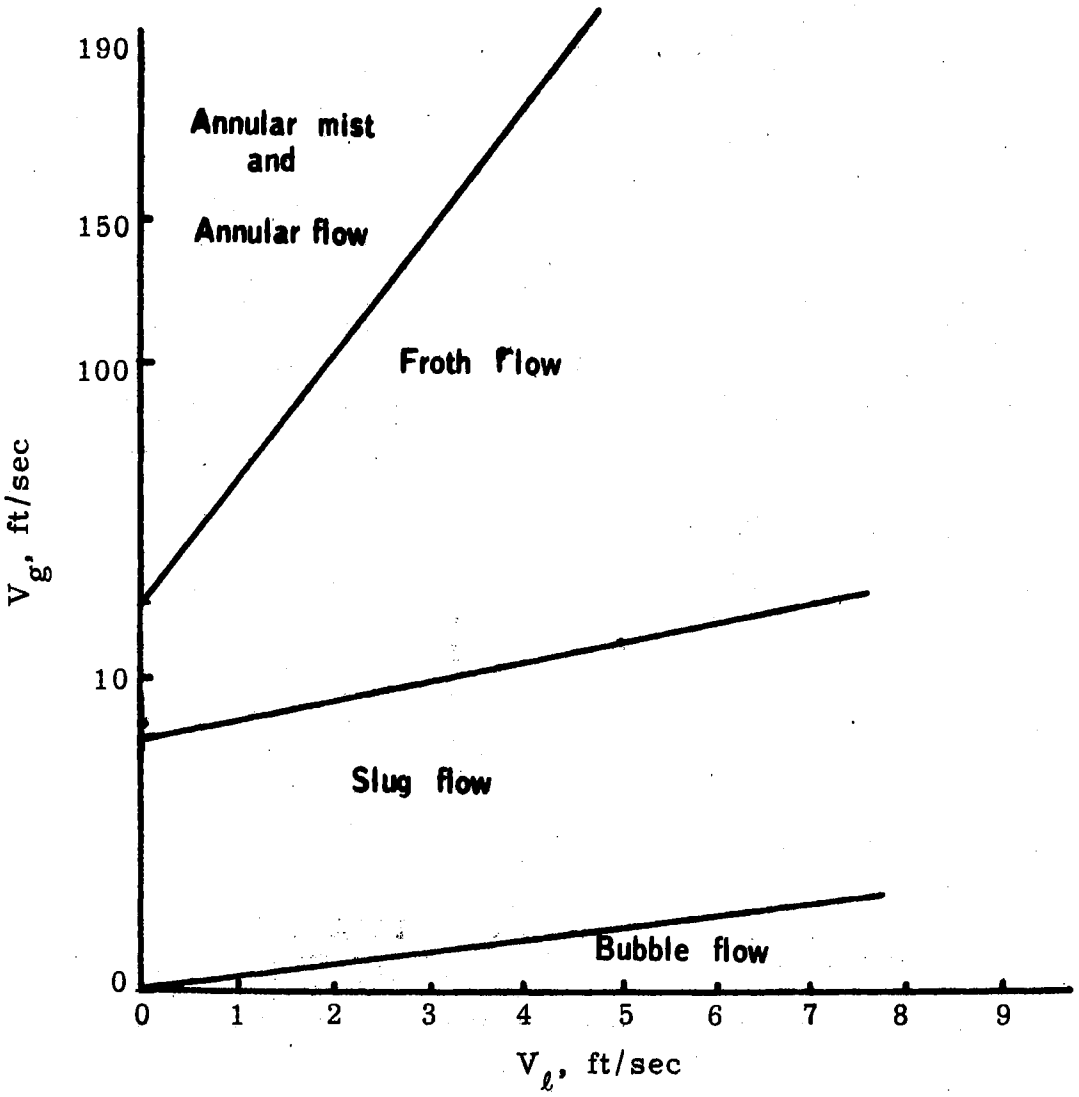

Figure 4. Vertical Upward Flow Map

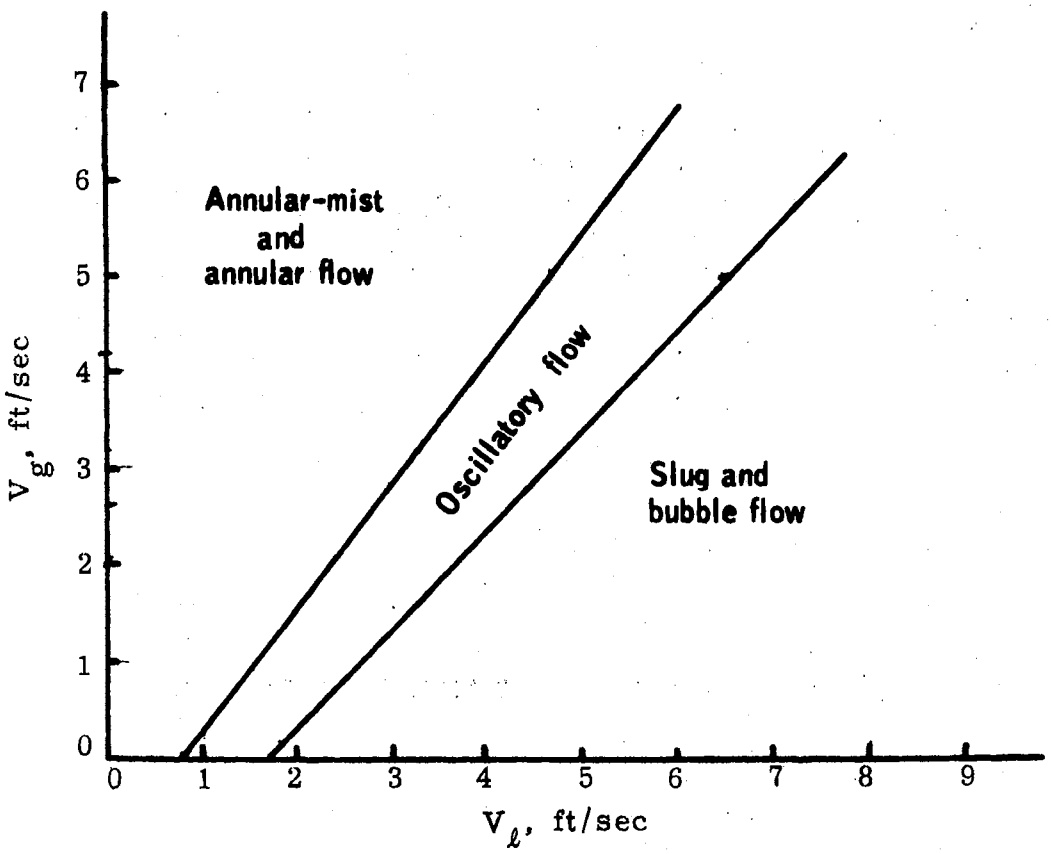

Figure 5. Flow Regime Map for Vertical Downward Flow

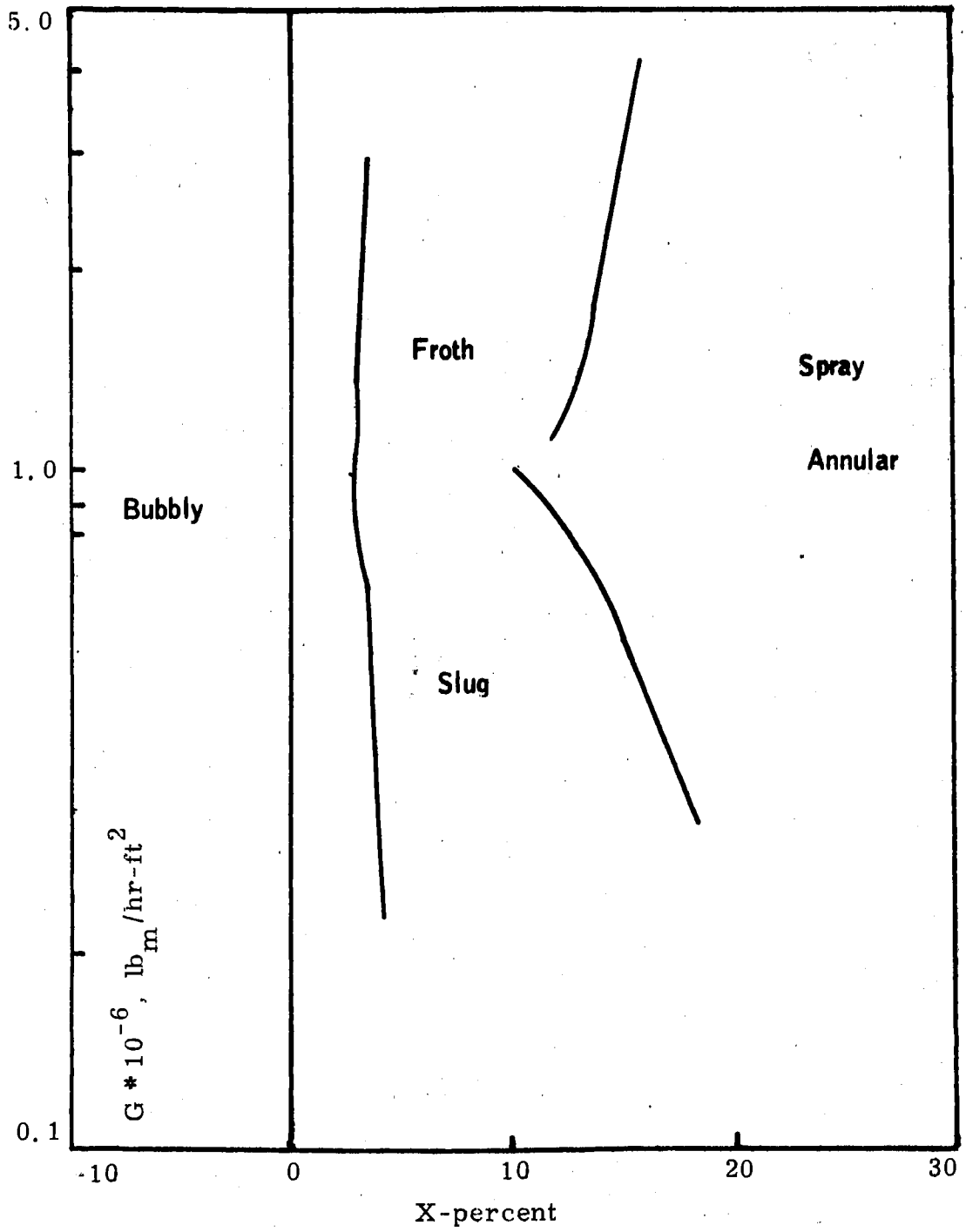

Figure 6. Typical Flow Regime Map Developed With Electrical Probe

$$R_v = \frac{x}{x + \frac{d_v}{d_\ell} s(1-x)} \qquad (2.8)$$

The ratio between the actual mean velocity of the gas and the liquid is called the slip ratio, s.

In this experiment we are considering adiabatic and isothermal flow and therefore the viscosity and density of air and water will remain constant. If we also consider fully developed flows and negligible vaporization, we can conclude that R_v will be constant for each run.

In this case we have

$$\left(\frac{\Delta P}{\Delta L}\right)_M = \left(\frac{\Delta P}{\Delta L}\right)_f + \frac{g}{g_c \Delta L}\left[d_\ell(1-R_v) + d_v R_v\right]\Delta h \qquad (2.9)$$

An estimate of the range of values of the terms are found in Appendix C.

Methods to correlate pressure drop fall into one of the four broad groupings:

1. Empirical correlations.

2. Models based on dimensional similarity or mathematical analysis, most of them included under the denomination of homogeneous models.

3. Semi-empirical approaches with physical models.

4. Numerical solutions to the energy, momentum and conservation equations.

Lockhart and Martinelli (20) propose four possible mechanisms during the simultaneous flow of a liquid and gas corresponding to the combinations of turbulent and laminar flows: liquid flow is laminar and gas flow is also laminar; liquid flow is turbulent and gas flow is laminar; liquid flow is laminar and gas flow is turbulent; and liquid flow is turbulent and gas flow is also turbulent.

They develop a semi-empirical correlation based on the assumptions that:

1. The static pressure drop for the liquid phase equals the static pressure drop for the gas phase regardless of the flow pattern, provided that an appreciable radial static pressure difference does not exist.

2. The volume occupied by the liquid plus the volume occupied by the gas at any instant equals the total volume of the pipe.

They define

$$\Phi_{V \text{ or } L} = \left[\frac{(dP/d\ell)_{f,\,TPF}}{(dP/d\ell)_{f,\,\ell \text{ or } v}}\right]^{\frac{1}{2}} \tag{2.10}$$

$$\chi = \left[\frac{(dP/d\ell)_{f,\,\ell}}{(dP/d\ell)_{f,\,v}}\right]^{\frac{1}{2}} \tag{2.11}$$

where $(dP/d\ell)_{f,\,v}$ and $(dP/d\ell)_{f,\,\ell}$ are the pressure gradients for the gas and liquid phases, respectively, flowing alone in single-phase flow within the channel. They presented four correlations of Φ versus χ corresponding to the four mechanisms. But the effects of geometry, methods of injection and pressure are considerable and are not taken into account completely.

To assess the effect of pressure, Martinelli and Nelson (21) developed a correlation of Φ versus χ_{tt} for the turbulent-turbulent mechanism, where

$$\chi_{tt} = \left(\frac{\mu_L}{\mu_v}\right)^{0.1} \left(\frac{d_v}{d_\ell}\right)^{0.5} \left(\frac{1-x}{x}\right)^{0.9} \tag{2.12}$$

Baroczy (3) tried to improve on Lockhart and Martinelli by defining a property index and two-phase multiplier, but this does not include

a correction for the surface tension which is probably the main reason for the deviation at high pressure.

Baker (22) considers the type of flow pattern when estimating two-phase pressure drop for the turbulent-turbulent mechanism. He also gives a method for correcting for hills when designing long distance pipelines.

Chenoweth and Martin (23) propose an empirical correlation for turbulent-turbulent flow. Here the two-phase pressure drop is assumed to depend on the flowing liquid volume fraction and pseudo-single-phase pressure drop.

Govier (5) presents a superficial friction factor in terms of the superficial water Reynolds number for various air-water volume ratios.

Brigham, Holstein and Huntington (24) present correlations between a pseudo-friction factor and a flow ratio to include the effects of uphill and downhill flow on pressure drop.

Jacowitz and Brodkey (25) have used a step-wise downstream method to predict pressure drop for the horizontal annular flow.

The homogeneous model assumes no slip between liquid and gas, i.e., the velocities of the liquid and gas are the same. This is not a good assumption. The frictional pressure drop is calculated by means of an equivalent single-phase mixture. The problem is in obtaining a satisfactory definition for single-phase mixture properties.

Woods' homogeneous model uses the following definitions:

$$\frac{1}{\bar{d}} = \frac{x}{d_v} + \frac{1-x}{d_\ell} \tag{2.13}$$

$$\frac{1}{\bar{\mu}} = \frac{x}{\mu_v} + \frac{1-x}{\mu_L} \tag{2.14}$$

Dukler, Wicks and Cleveland (26) have proposed a new approach to correlate frictional pressure drop in two-phase flow based on a similarity analysis. They consider two flow systems that are dynamically similar. Therefore, they can establish the conditions of kinetic and geometric similarity for two points located at geometrically similar positions relative to the boundaries. Once they relate the local quantities to space average ones, they obtain the parameters for two-phase flow corresponding to the Euler and Reynolds numbers for single-phase flow.

An important conclusion is that for such a system the definitions for mixture density and mixture viscosity are no longer arbitrary.

Dukler et al. consider four special cases and state that by properly selecting values for the grouping variables it is possible to develop either the friction factor or the Reynolds number expression used by many, if not all, of the previous investigators.

They have experimentally checked two cases and compared the results of their model with those obtained with the Lockhart-Martinelli model. As methods for predicting hold-up are improved, those results should be even more satisfactory.

Visual Study Techniques

The methods used in visual studies of two-phase flow are indicated in Figure 7.

In direct illumination photography, the subject is illuminated from the side on which the camera is located. The light is either reflected toward the camera or refracted away from it, depending upon the nature

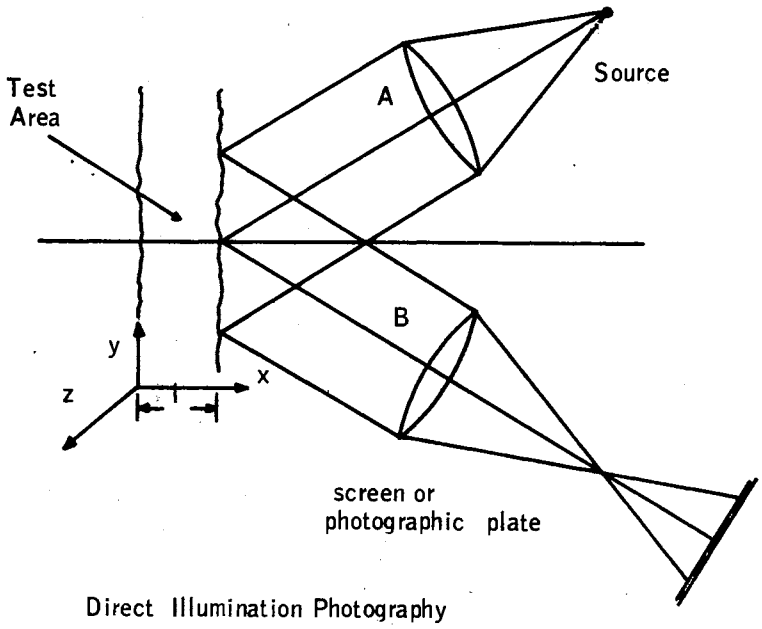

Direct Illumination Photography

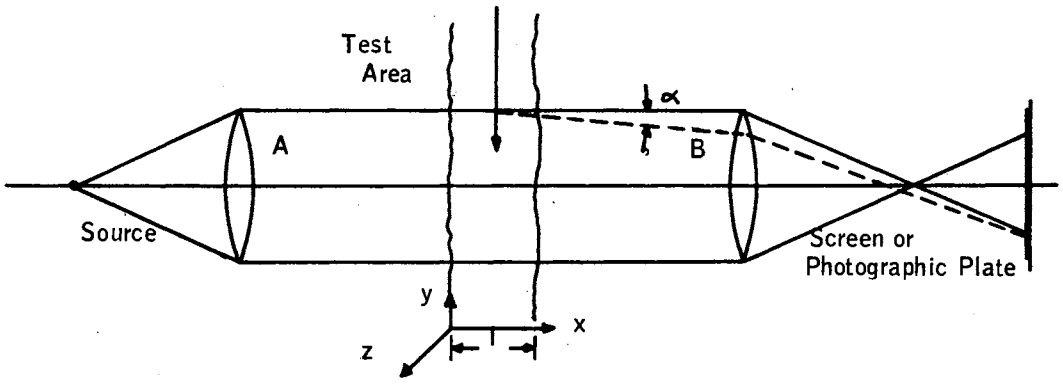

Shadow-graph Photography

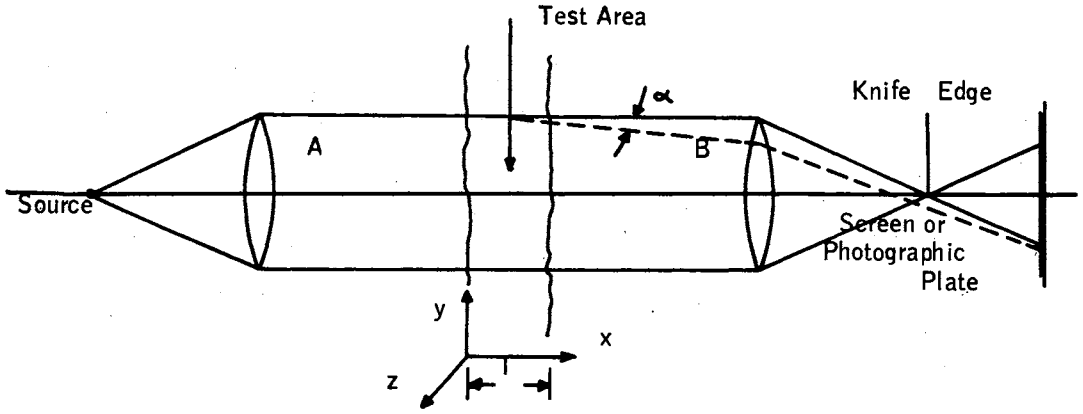

Schlieren Photography

Figure 7. Various Photography Techniques

of the surface at the illuminated point. Surface disturbances are thus highlighted on the film.

Shadowgraph and schlieren photography have as a basic operating principle the detection of density gradients which will produce a non-uniform bending of the light which therefore produces a non-constant illumination of the screen.

The three methods are distinguished by the optical paths of the light.

The selection of camera and film is normally accomplished by a compromise between resolution and speed. The most popular camera is the 16mm rotating prism movie camera, operating at variable speeds from 300-10,000 frames per second.

The sources of light are photoflood tungsten iodide or mercury vapor lamps.

CHAPTER III

EXPERIMENTAL APPARATUS

General Assembly

Figure 8 gives a flow scheme of the experimental setup. The system used in this study was air and water. The apparatus consisted of a 1-inch ID, 12 feet long, glass pipe mounted on a wooden board on an angle iron frame which could be adjusted to various inclinations. After passing through control valves and metering instruments, the fluids entered the test section through a standard 3/4*3/4*3/4 inch screwed tee connection as shown in Figure 9.

The air line consisted of a 3/4-inch ID schedule 40 pipe with two rotameters in parallel capable of measuring up to 10.45 ft^3/min each, and two 3/4-inch globe valves to regulate the flow on each branch. At the outlet of each rotameter there were two 3/4-inch check valves to prevent water getting inside the rotameters.

The water line was a 3/4-inch ID schedule 40 pipe with a globe valve to regulate the amount of water required. Although an orifice meter was installed in the line to measure the flow rates, the meter was not used because it was considered to be more accurate to direct the flow to a container on a scale where the weight of water existing during a given time period was measured and converted into gal/min. This time period depended on the flow rate of water which varied from 1 to 10 minutes. The range of water flow rates was 0-10 gal/min.

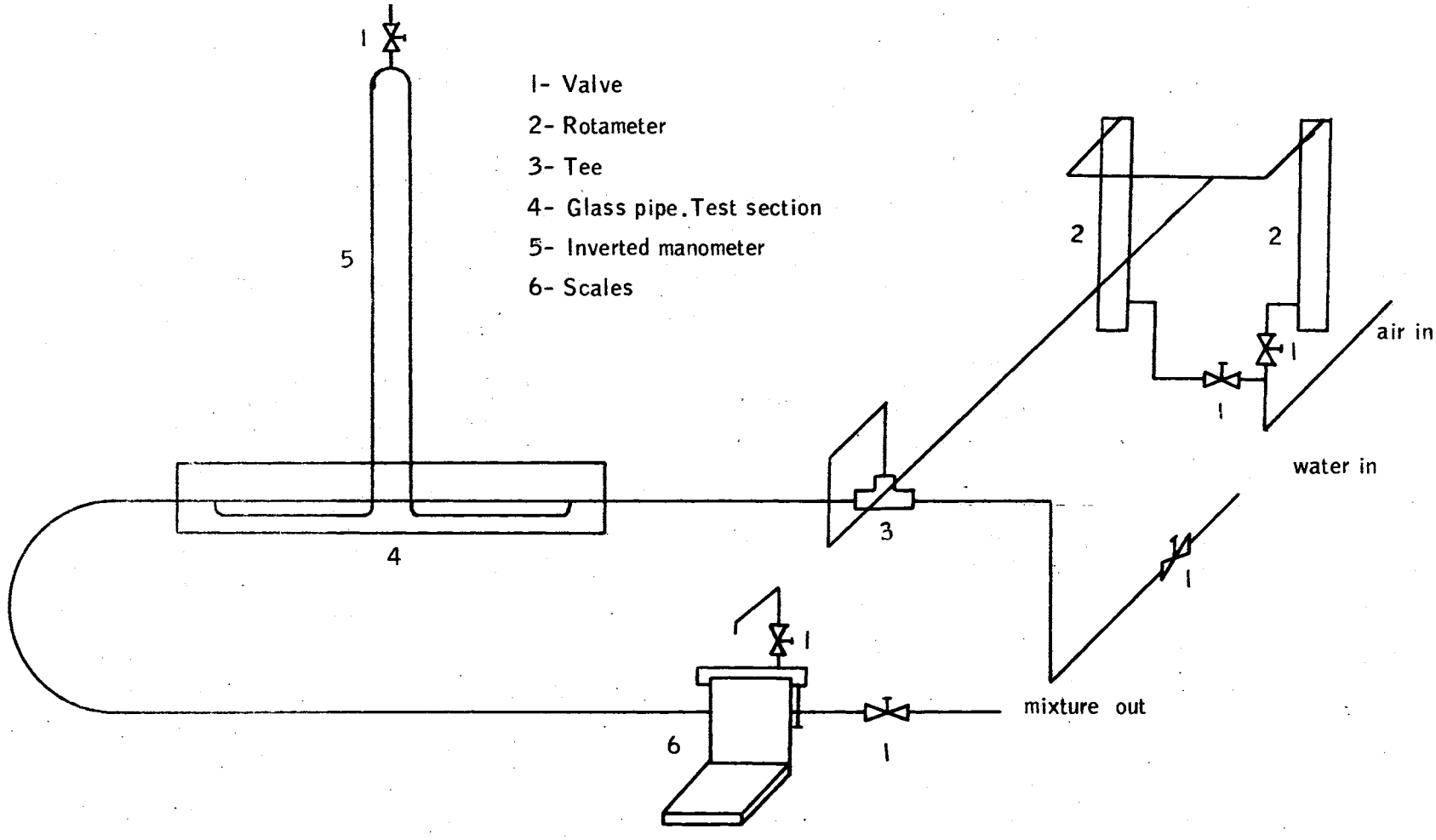

Figure 8. Schematic Diagram Showing Flow System

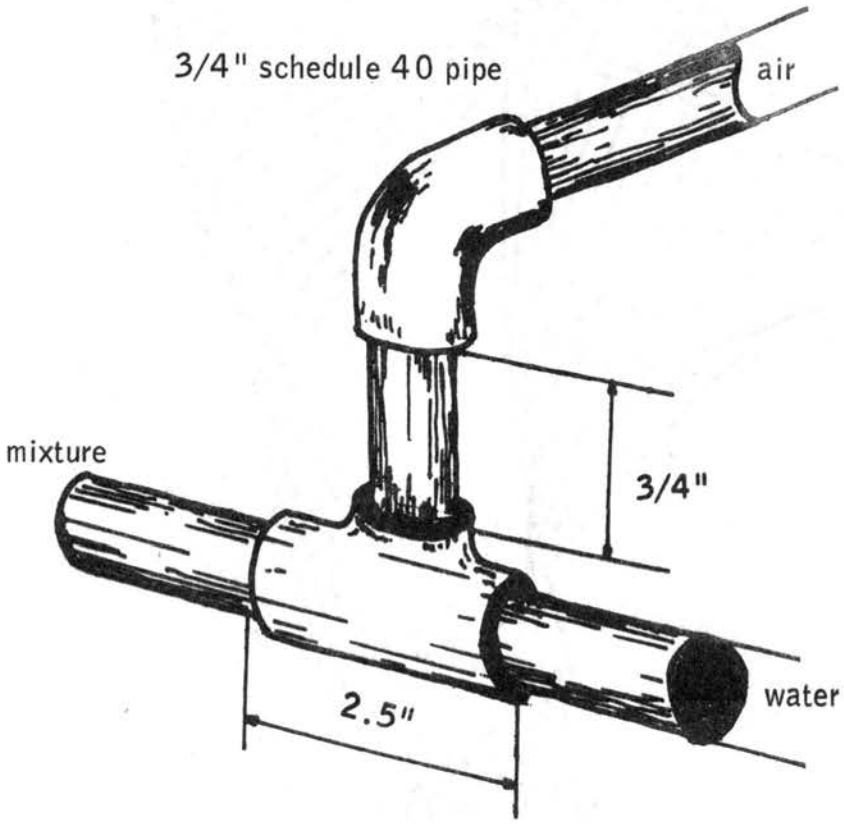

Figure 9. Mixing Tee

Liquid and gas were fed simultaneously to the test section through a standard 3/4*3/4*3/4-inch screwed pipe tee connection with the liquid entering the run and the gas entering vertically downward through the branch.

The connection from the 3/4-inch pipe to the 1-inch ID glass pipe was made with a 1-inch ID plastic tube and hose clamps. The distance between the mixing tee and the entrance to the glass pipe was three feet.

The test section consisted of the glass pipe and the manometer.

The glass pipe was 12 feet long with two 1/4-inch ID pressure taps welded 10 feet apart and connected with 1/4-inch ID plastic tubing to a manometer. Since the presence of two phases in the manometer lines can cause serious errors, the pressure taps were situated at the bottom of the pipe to avoid air bubbles in the manometer lines.

Mechanically induced vibrations transmitted to the test section could affect the pressure drop readings strongly and increase the risk of breaking the glass pipe. For this reason the glass pipe was mounted on a 12-foot board which was six inches wide and one-half inch thick. Rubber-cushioned bolts at two-foot intervals fastened the glass pipe to the board. Plastic-pipe connections were used upstream and downstream of the glass pipe. Thus the pipe did not move during fluctuating flow.

The air-over-water manometer was an eight-foot inverted U-tube made of 1/4-inch ID glass tubing mounted on a nine-foot board. In this way it was possible to obtain a larger scale for reading and at the same time it was safe in the event of a high pressure drop which could throw out the manometric fluid.

There was a stopcock valve ontop of the inverted U-tube manometer to purge the air bubbles in the lines and to eventually displace the level of water to facilitate the readings.

The two-phase flow was directed either to the drain or to a container on a scale to measure the flow rate of water.

Photography

In close-up photography correct focusing of the subject comes first; at the same time, some depth of field is required. While in the experiment the plane passing through the center of the glass pipe was considered the main subject, it was intended to have a depth of field for the whole glass pipe as well, so that blur would be negligible in this zone.

This could be done by varying three factors which can be adjusted independently or in combination:

1. Focal length of the lens, so we would use a wide angle lens to get more depth of field. In the experiment a normal f:50mm Nikkor-H Auto 1:2 lens was used.

2. The lens-taking aperture should be a small one and a high shutter speed should be used. In the experiment a shutter speed of 1/1000 second and lens apertures of f/2.8 and f/3.5 achieved the best results.

3. Lens to subject distance: this would imply using special close-up lenses. Good focus can be achieved by increasing the magnification power of the lens through the attachment of a supplementary lens to the camera lens or by extending the lens to film distance through the inser-

tion of a device of a fixed (ring) or adjustable (bellows) length between the lens and the camera body.

In this experiment pictures were taken with a Nikon F camera provided with a waist-level Finder, and a f:50mm Nikkor-H Auto 1:2 lens with a polaroid filter to minimize reflections in the glass. The camera was provided also with a K-1 extension ring to give a greater depth of field and magnification. The pictures were focused on the middle of the pipe with black paper for background. The camera was mounted on a tripod to keep the camera steady and a cable release was employed. Kodak Tri X film was used.

For a future study it would be better to use a 55mm f/3.5 Micro-Nikkor-P Auto with the M-2 ring and strobe flash or a 200mm f/5.6 Medical-Nikkor Auto.

CHAPTER IV

EXPERIMENTAL PROCEDURE

In each run the following readings were taken: Air and water flow rates; maximum, minimum and average pressure drops; visual observations of the flow regimes involved; and photographs of the typical flow regimes. These data were obtained for the isothermal and adiabatic two-phase flow of water and air mixtures at near room temperatures.

For each inclination of the glass pipe several series of runs were made. In each series the flow rate of water was kept constant while the amount of air was varied from 0 to 20.90 ft^3/min in such a way as to obtain data points showing a clearly defined flow pattern. Thus, in the case of a transition line being found the zone represented by this transition line could be limited between two data points.

Before taking any data, ample time was allowed on each run to insure steady-state conditions. The time varied from 5 to 25 minutes depending on the flow rates involved.

In each series one run was repeated to insure the same readings, but in the slug flow regime the reproducibility was not always good.

With some flow regimes, reading the rotameters and manometers was difficult due to pulsations. In order to avoid these pulsations, both rotameters were provided with globe valves which helped to eliminate the fluctuations by allowing the same amount of air to pass through each rotameter. For the same reasons, three readings were taken in the

manometers corresponding to maximum, minimum and average pressure drops observed during a given run. Although for some runs with no fluctuations only one pressure drop reading was sufficient, for other runs two pressure readings were taken because the maximum or minimum pressure drop reading was assumed to be the same reading as the average one.

It was observed that for low flows of water the inlet mixing tee and wall effects were factors to be considered in the analysis of the results. This is because the stratified flow regime is unstable in such a way that if there is any irregularity in the pipe, such as those produced by the pressure taps or by a slight dip, waves will be produced.

The connection between the 3/4-inch pipe and the test section was made with plastic pipe so that if a bend was formed in the plastic pipe, water could accumulate and be blown up periodically by the upcoming air producing a slug. Inadequate mixing is caused by the mixing tee, because the water goes preferentially to the bottom of the pipe while the lighter air remains on top of the pipe.

Special precautions were taken against air getting inside the manometer lines; two stopcock valves were used in the 1/4-inch plastic tubing line to decrease the effective diameter of the line for the air bubbles.

Photographs were taken with a shutter speed of 1/1000 second to stop the action as much as possible. The best lens apertures were f/2.8 and f/3.5.

CHAPTER V

REPRESENTATION AND DISCUSSION OF RESULTS

The pressure drops in the pipe were calculated using the following equation and a picture of the system is shown in Figure 10.

$$\Delta P_1 = \left[\frac{\Delta h}{12}(d_\ell - d_v) - \frac{d_\ell}{12}(h_1 - h_2)\right]/10.0 \qquad (5.1)$$

where

Δh = manometer indication, inches

d_ℓ = density of water, 62.3 lb_m/ft^3

d_v = density of air, 0.08071 lb_m/ft^3

h_1 = height of pressure tap 1, inches

h_2 = height of pressure tap 2, inches

ΔP_1 = pressure drop between points 1-2, psf/ft length.

When Baker (2) presented his results, he used $G_\ell \lambda \bar{\Psi}/G_V$ as the abscissa and G_V/λ as the ordinate. In this text, however, a transformed Baker flow regime map will be used to present the results defining the ordinate, y, as G_V/Λ and the abscissa, x, as $G_\ell \Psi$.

The transformed Baker map coordinates have been calculated as follows:

$$\Lambda = \sqrt{d_\ell d_v} = \sqrt{62.3 * 0.08071} = 2.24 \ lb_m/ft^3 \qquad (5.2)$$

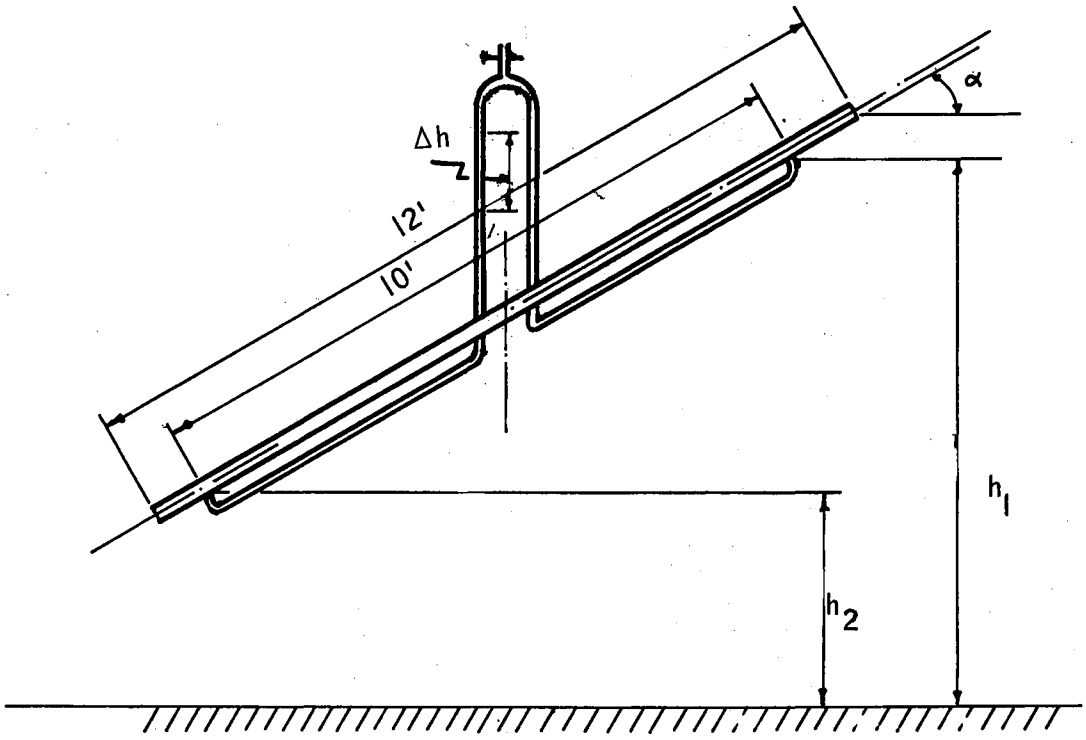

Figure 10. Manometer System

$$\psi = \frac{\mu_L^{\frac{1}{3}}}{\sigma\, d_\ell^{\frac{2}{3}}} = \frac{(2.42)^{\frac{1}{3}}}{73 * (62.3)^{\frac{2}{3}}} = 0.001172 \frac{\text{cm-ft}^{5/3}}{\text{dyn-hr}^{\frac{1}{3}}\text{-lb}_m^{\frac{1}{3}}} \qquad (5.3)$$

$$V_v = (y\Lambda\ \text{lb}_m/\text{h-ft}^2)\,(S\ \text{ft}^2)\left(\frac{1}{d_v\ \text{lb}_m/\text{ft}^3}\right)\left(\frac{1\text{h}}{60\ \text{min}}\right)$$

$$= y * 2.24 * 0.005454 * \frac{1}{0.08071 * 60}$$

$$= 2.5228 * 10^{-3}\, y\ \text{ft}^3/\text{min} \qquad (5.4)$$

$$V_L = \times \frac{1}{\psi}\ \text{lb/h-ft}^2\,(S\ \text{ft}^2)\,\frac{1}{d_\ell\ \text{lb/ft}^3}\ \ \frac{1\text{h} * 1\ \text{gal}}{60\ \text{min} * 0.13368\ \text{ft}^3}$$

$$= \times \frac{1}{0.001172} * 0.005454 * \frac{1}{62.3 * 60 * 0.13368}$$

$$= 9.304 * 10^{-3} * x\ \text{gal/min} \qquad (5.5)$$

So that the actual data readings of air and water flow rates can be converted to the coordinates which will be used in the presentation of the results, the coordinates y and x corresponding to certain air and water flow rates are given:

x-y	10^0	10^1	10^2	10^3	10^4	10^5
Air ft^3/min			$2.52*10^{-1}$	$2.52*10^{0}$	$2.52*10^{1}$	$2.52*10^{2}$
Water gal/min	$9.3*10^{-3}$	$9.3*10^{-2}$	$9.3*10^{-1}$	$9.3*10^{0}$	$9.3*10^{2}$	$9.3*10^{2}$

(5.6)

All the calculations were performed with a Friden electronic calculator and the results are given in Appendix D.

The experiment was divided into three parts corresponding to horizontal pipe, pipe inclined 5°, and pipe inclined 15°.

Horizontal Pipe

This series of runs was made in order to have a basis to compare with the transformed Baker flow regime map (27).

A total of 106 points was measured. These were distributed in nine series; in each series the flow rate of water was kept constant while the air flow rates were varied. The water flow rates ranged from 0.041 to 7.986 gal/min while the air flow rates ranged from 0.0 to 20.9 ft^3/min.

The transformed Baker flow regime map as indicated by the present results is shown in Figure 11. It is necessary to clarify that the line of separation between wavy and annular regions is difficult to draw because the wall effect, mixing tee and external configuration of the system play an important role. Comparison with the transformed Baker's map indicates that this line, wavy-annular, is almost a horizontal line and tends to intersect the ordinate axis at $G_v/\Lambda = 10^4$.

The separation line between plug and slug is not so steep compared to Baker's transformed map. Also, it is displaced upward giving a larger plug region.

The separation line between slug and annular region is not as curved as in the transformed Baker's map, but otherwise it is drawn at approximately the same ordinates as in the transformed Baker's map.

The boundary between stratified-plug-slug-wavy-annular regions is not clear and there exists the possibility that the wavy region should extend to the x-axis.

The wall effect region can be limited to $G_\ell \Psi < 1.5 * 10^1$ where the stratified region is influenced by the mixing tee wall effects and external configurations. Thus, the results are not clear in that region.

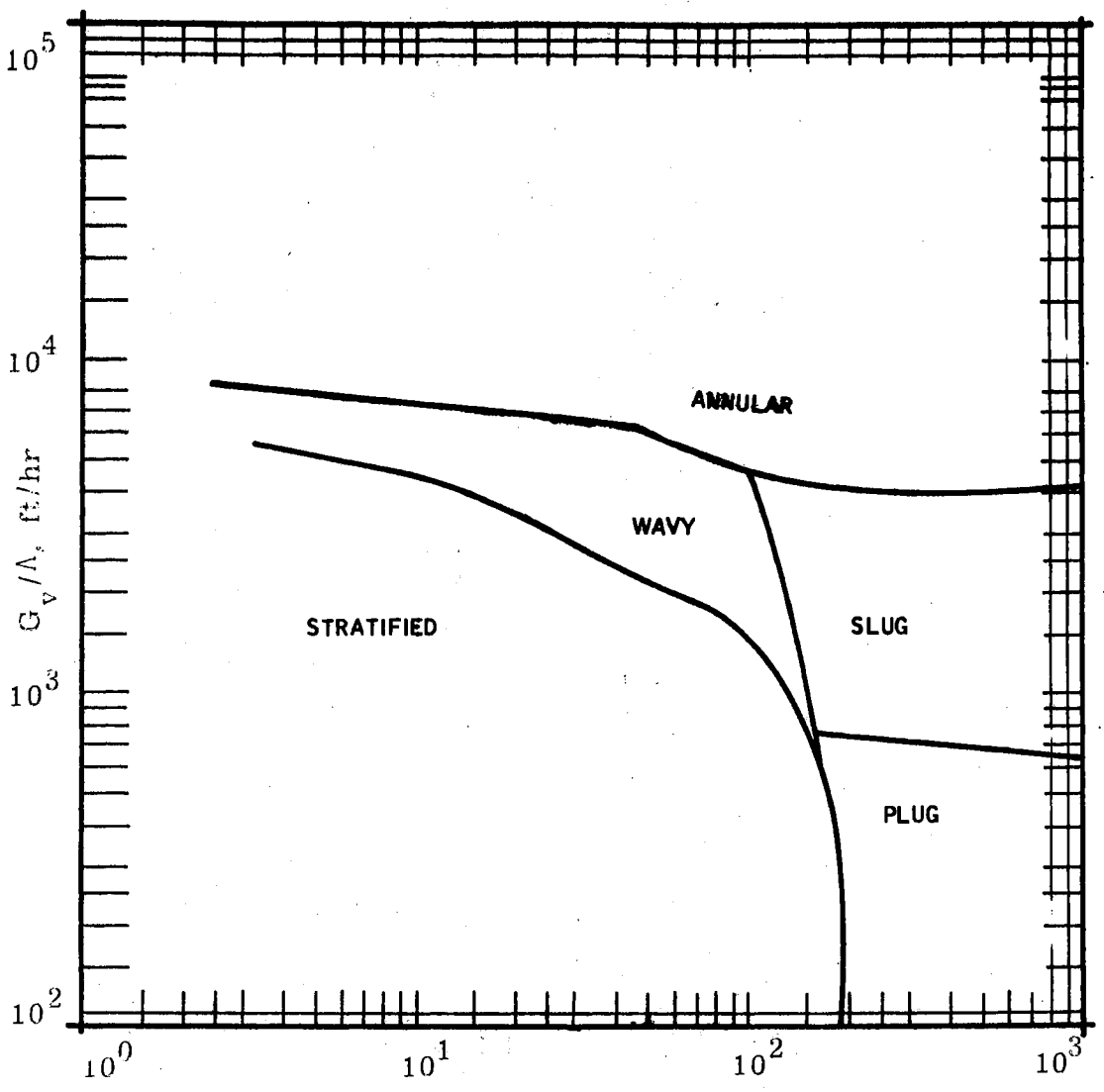

Figure 11. Modified Baker Map for Horizontal Pipe

A new and probably better method of presenting the results is shown in Figure 12, where the pressure drop in psf/ft of length is given together with the flow pattern regions for the nine series of runs. The pressure drop is the ordinate and G_v/Λ is the abscissa while $G_\ell\psi$ is the variable parameter.

In some runs it was necessary to take three pressure drop readings corresponding to a maximum, minimum and average, while in other instances two readings or, when there was no oscillation, even one reading would suffice. In Figure 12 only the average pressure drop readings are shown.

From the results it can be seen that for $G_\ell\psi = 4.35 * 10^0$ and $G_\ell\psi = 1.24 * 10^1$; only one reading was necessary. Since it was in the wall effects region, readings were taken through the stratified, wavy and annular regions. The results are given in Appendix D.

$G_\ell\psi = 2.05 * 10^1$, $G_\ell\psi = 2.36 * 10^1$ and $G_\ell\psi = 3.6 * 10^1$ show little oscillation of the pressure drop. This series of data points was taken in the stratified, wavy and annular regions.

$G_\ell\psi = 9.0 * 10^1$ shows some points with great oscillations. This is a clear indication that they are in the transition line from wavy to slug flow regime.

$G_\ell\psi = 1.7 * 10^2$ and $G_\ell\psi = 3.65 * 10^2$ show points with great oscillations even with negative pressure drop readings. The system goes from plug region to slug region and finally to annular. In the annular region, the three readings tend to join in only one point. It can be seen also that the oscillations in the plug flow regime are not as great as in the slug regime.

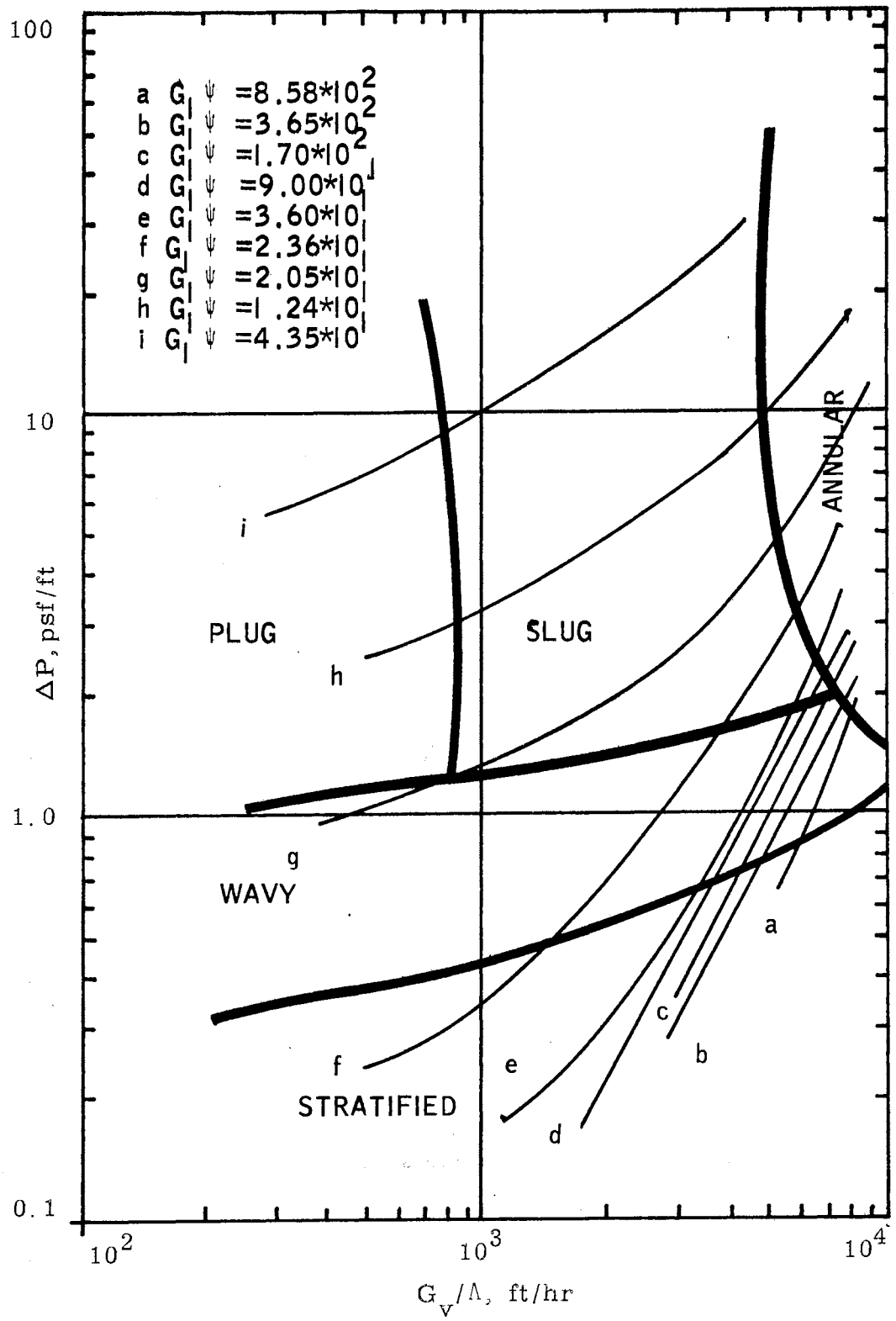

Figure 12. Pressure-Flow Pattern Map for Horizontal Pipe

$G_{\ell\psi} = 8.58 * 10^2$ shows that the oscillations in the slug regime are not as great as before. This could be interpreted as being due to the fact that the air cannot produce a fast speed slug with the high flow rates of water.

Comparing all the results, it can be said that the pressure drop increases with increasing flow rate of water and also that the pressure drop increase is greater at larger flow rates of water. This increase in pressure drop is due not only to the larger amount of liquid being transported, but also is a result of the decreased flow area open to the gas phase and of irreversible work performed on the liquid by the gas.

It can be concluded that the stratified and wavy regions will give a low pressure drop while the plug, slug and annular regions will give a high pressure drop which will be higher at increasing water flow rates.

Pipe Inclined 5° Downward Flow

In this series of runs a total of 114 points was measured. These were distributed in 11 series. In each series the flow rate of water was kept constant while the air flow rate was varied.

The water flow rates ranged from 0.077 to 8.11 gal/min while the air flow rates varied from 0.0 to 20.9 ft^3/min.

The Baker type flow regime map as indicated by the present results is shown in Figure 13. This figure primarily demonstrates that the wavy region has increased in size while the plug and slug regions have decreased. A decrease in the stratified region would have been expected because now the gravity force acting on the two-phase flow has decreased in proportion to the cosine of the angle of orientation to the

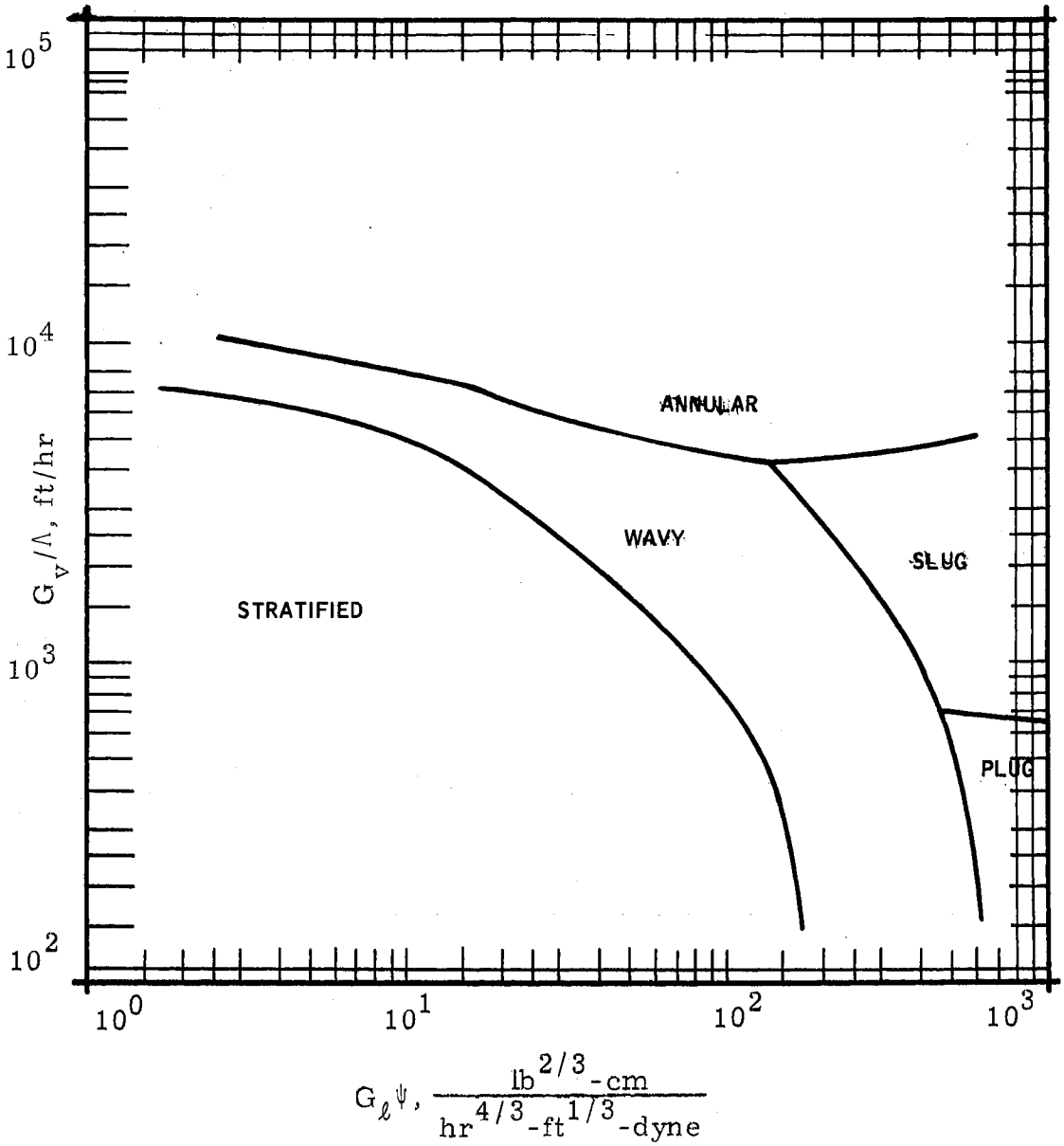

Figure 13. Baker Map for Pipe Inclined 5°

vertical and therefore the stratified flow, which is totally gravity controlled, should be more influenced, thus giving a smaller stratified region.

As shown previously, the transition line from wavy to annular seems to be more similar to a horizontal line than to what Baker originally illustrated in Baker's transformed map.

The plug-slug line also appears to be more similar to a horizontal line than in Baker's map and it has the same ordinates as we found in the horizontal pipe.

There are indications of change of flow regimes with length. This was occasionally seen in the following cases: (1) Annular at the inlet going to slug at the outlet of the pipe; (2) plug going to wavy; (3) wavy going to stratified. Although this appears to be a sound theory, there is not positive confirmation that this actually happens.

Figure 14 shows the probable flow pattern regions together with the average pressure drop readings in psf/ft length. The pressure drop is the ordinate and G_v/Λ is the abscissa, while $G_\ell\psi$ is the variable parameter. In some runs it was necessary to take three pressure drop readings corresponding to a maximum, minimum and average; in other instances two readings were sufficient or even one reading when there was no oscillation.

To help to interpret the results, an oscillation is going to be considered when there is at least two inches of water variation between maximum and minimum readings; this is equivalent to 1.05 psf/ft.

In general it can be said that the results do not correlate as well as in the horizontal case, because there are more irregular oscillations.

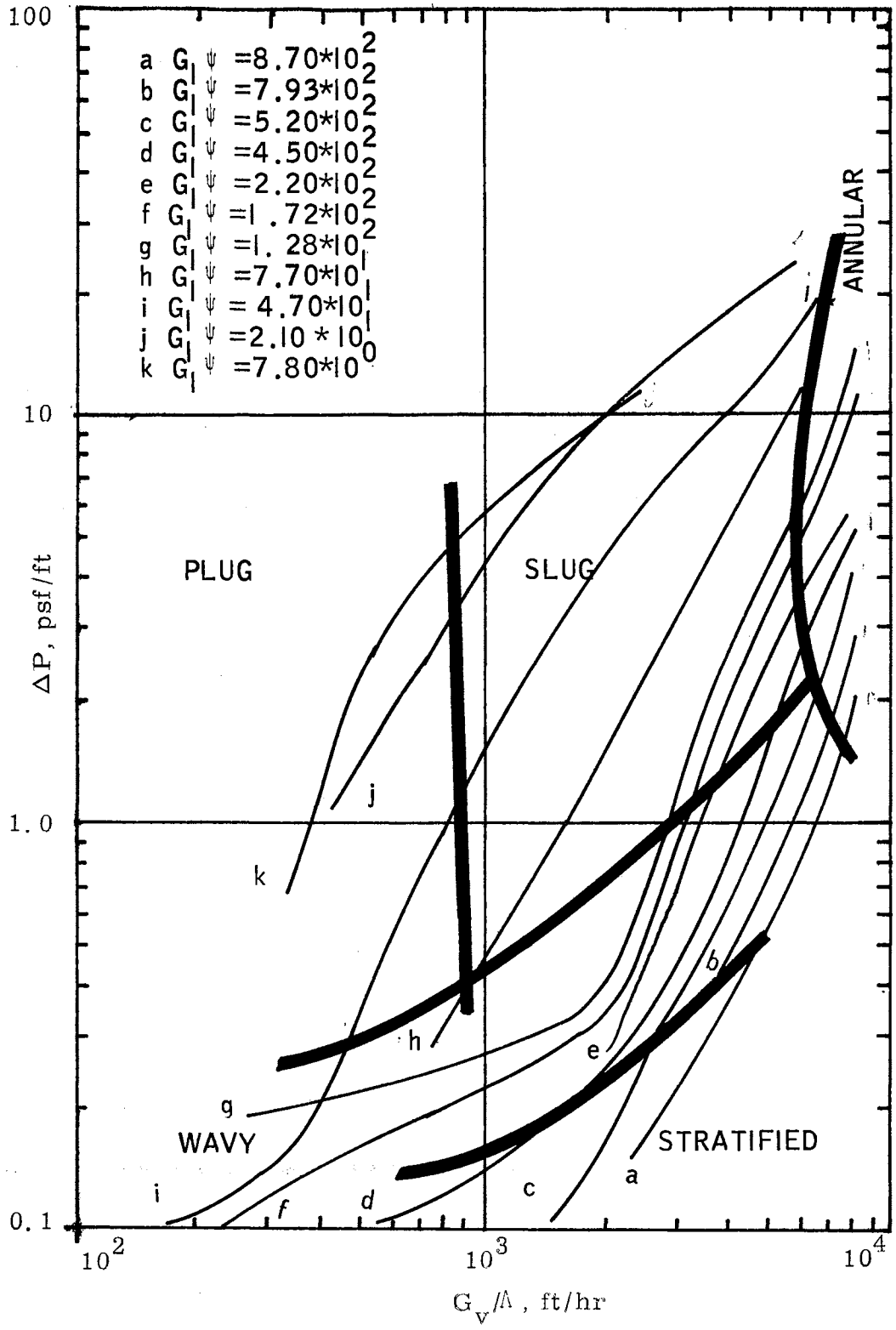

Figure 14. Pressure-Flow Pattern Map for Pipe Inclined 5°

$G_{\ell}\psi = 7.8 * 10^{0}$, $G_{\ell}\psi = 2.1 * 10^{1}$, and $G_{\ell}\psi = 4.7 * 10^{1}$ show that only one reading was required to take in the manometer. The data points are found in the stratified, wavy and annular regions.

$G_{\ell}\psi = 7.7 * 10^{1}$, $1.28 * 10^{2}$, $1.72 * 10^{2}$, $2.2 * 10^{2}$ show little oscillation and it can be concluded that the oscillations were found in points in the boundary with the slug region; otherwise the points are found in the stratified, wavy and annular regions.

$G_{\ell}\psi = 4.5 * 10^{2}$, $5.2 * 10^{2}$, $7.93 * 10^{2}$ and $8.7 * 10^{2}$ show great oscillations which can be interpreted as points found in the plug, slug and finally the annular regions.

As previously found, the wavy and stratified regions give low pressure drop; now, however, part of the plug region also gives a small pressure drop while the upper part of the plug region and the slug and annular regions give a high pressure drop.

Pressure drop is higher at higher water flow rates.

The pressure drop lines are very steep at low $G_{\ell}\psi$ and the slope of these lines decreases as this parameter $G_{\ell}\psi$ increases.

Pipe Inclined 15° Downward Flow

In this series of runs a total of 133 points was measured. They were distributed in 15 series. In each series the flow rate of water was kept constant while the air flow rate was varied.

The water flow rates ranged from 0.060 to 5.124 gal/min while the air flow rates varied from 0.0 to 20.9 ft^{3}/min.

The transformed Baker flow regime map as indicated by the present results is shown in Figure 15. This figure shows that there is a displacement to the left in the map so that the slug region increases

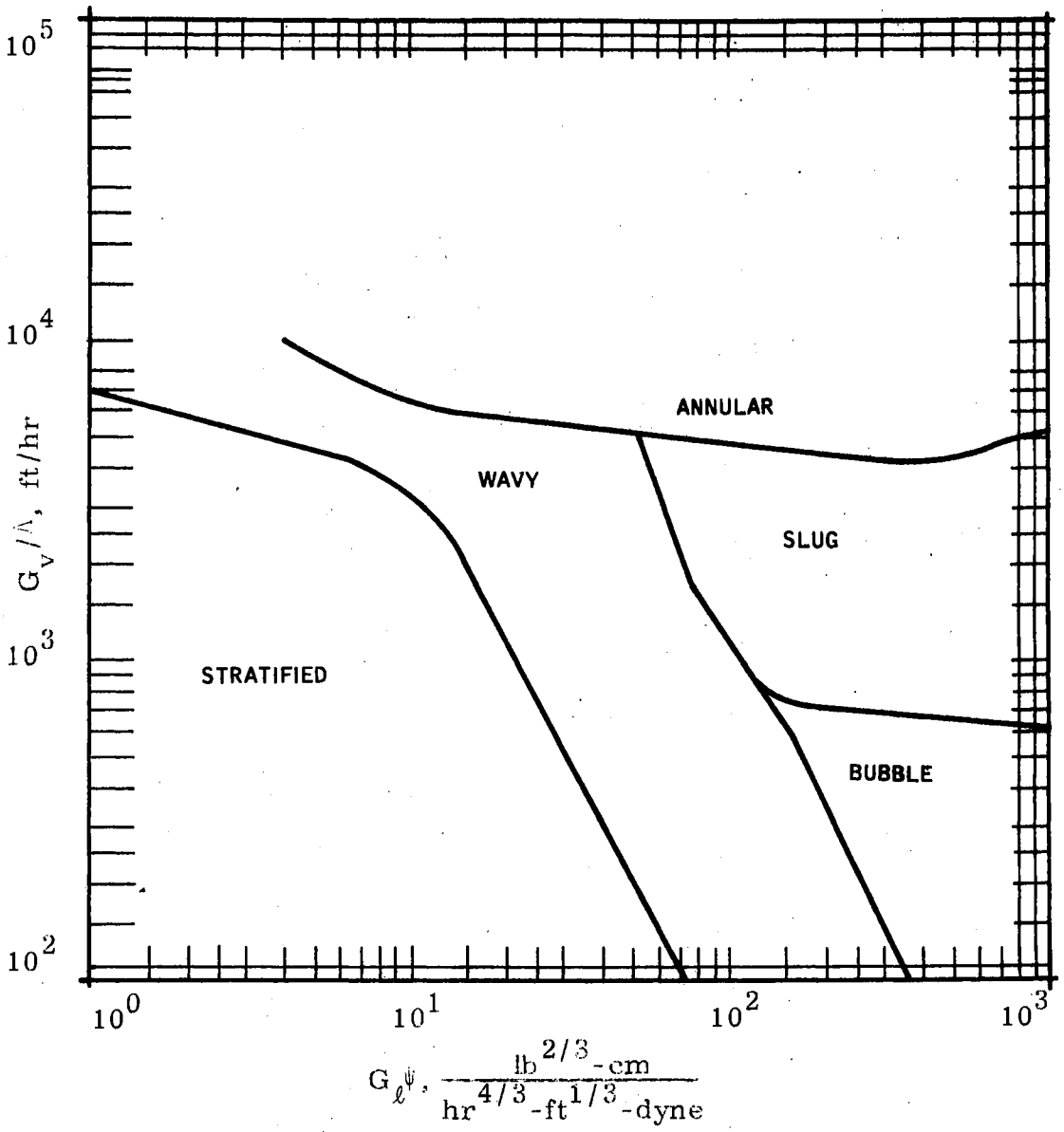

Figure 15. Baker Map for Pipe Inclined 15°

in size, the wavy region remains the same and the stratified region is decreased. If the boundary line between stratified and wavy regions were extended, it would intersect the x-axis at $G_\ell\psi = 7 * 10^1$, while the wavy-bubble boundary line would intersect at $G_\ell\psi = 3 * 10^2$.

The plug flow as it was defined previously does not appear and there is a new type of flow which will be considered as bubble flow. Small plugs are found dispersed through the top of the liquid, and therefore, it is reasonable to assume that what is plug flow at the inlet of the pipe becomes bubble flow at the outlet and that with a slightly greater inclination, only the bubble flow would be found.

On the other hand, the line of separation between this new bubble zone and the slug zone occurs at ordinates of $G_v/\Lambda = 7.5 * 10^2$, or the same as it was in previous cases.

Also $G_\ell\psi < 1.5 * 10^1$ may be considered the zone where the wall, mixing tee and external effects are important.

The line of separation between slug and annular zones remains at the same ordinates.

Another finding is the confirmation of change of flow regimes with length. In addition to plug going to bubble, it was also observed that annular flow at the inlet of the test section becomes slug at the outlet.

There were some indications, without a positive confirmation, of wavy going to slug flow and of wavy going to stratified flow. It could be confirmed with greater length and without external effects due to mixing.

Another observation is that for the high air flow rates there are indications of changes in the conventional annular flow regime. One change is that the liquid film on the wall becomes milkier in color. This

could be because of the higher air flow rates or because part of the liquid is becoming entrained in the core gas.

Figure 16 shows the results of average pressure drop readings and flow patterns presented together in a single figure. The average pressure drop in psf/ft length is the ordinate, G_v/Λ is the abscissa, while $G_\ell\psi$ is the variable parameter.

In some runs it was necessary to take three pressure drop readings corresponding to a maximum, minimum and average, and in other cases two readings or, when there was no oscillation, even one reading sufficed.

An oscillation will be considered when there is at least two inches of water variation between maximum and minimum readings. This is equivalent to 1.05 psf/ft.

$G_\ell\psi = 6.45 * 10^0$, $1.39 * 10^1$, $1.97 * 10^1$ show no practical fluctuation. The data points are found in the stratified, wavy and annular zones.

$G_\ell\psi = 4.24 * 10^1$ shows in the first four points oscillations which would not be expected. The reading for the average pressure drop is higher than in subsequent series. This could be explained as the effects of the mixing tee, etc., or as a result of the transition zone approaching.

$G_\ell\psi = 6.06 * 10^1$, $8.0 * 10^1$, $9.7 * 10^1$, $1.09 * 10^2$ show consistently in the first points a small oscillation. This is an indication that these points are in a modified wavy zone because the transition line with the slug and bubble zone is very close.

$G_\ell\psi = 1.60 * 10^2$, $1.96 * 10^2$, $2.28 * 10^2$, $3.34 * 10^2$, $3.87 * 10^2$, $4.68 * 10^2$, $5.5 * 10^2$ show the typical oscillations of at least 1.05 psf/ft of the slug flow regime.

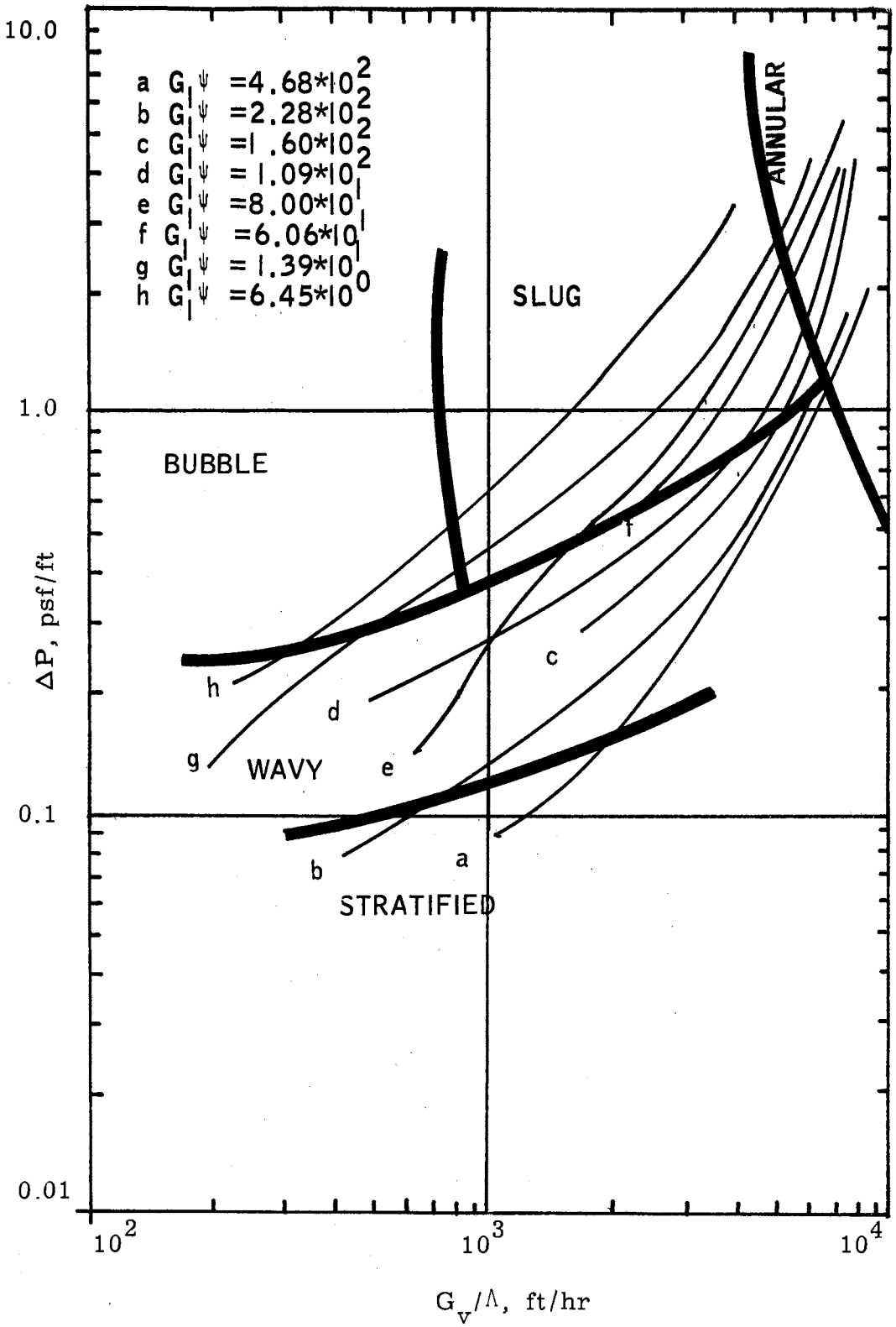

Figure 16. Pressure-Flow Pattern Map for Pipe Inclined 15°

It can also be seen that $G_{\ell}\psi = 2.28 * 10^2$ gives higher average pressure drop readings than subsequent series of readings. There is no explanation for this behavior unless the difficulty of the experimental readings made them inaccurate.

In general the pressure drop measurements do not correlate as well as in the horizontal case because oscillations are greater and more frequent. There are some points with negative pressure drop readings for the minimum value. Those occur especially in the slug zone for low air flow rates.

The oscillation shown in the stratified zone occurs because in this so-called wall effect zone, the stratified flow regime is unstable and from time to time a slug is superimposed in the stratified flow due to the external effects, mixing tee and plastic connections, producing the oscillation in the pressure drop reading.

In general it can be said that the pressure drop increases as the water flow rate increases but this does not occur as regularly as in the horizontal case or even in the 5° inclination pipe case.

The wavy and stratified region present a low pressure drop but now that the stratified zone has been reduced, it can be seen that part of the bubble and slug zone have also a low pressure drop and that the zone of the high pressure drop is occupied by the bubble, slug and annular regions.

CHAPTER VI

CONCLUSIONS AND RECOMMENDATIONS

Conclusions

The general conclusions from this study are as follows:

1. In our configuration the stratified zone is greatly influenced by external and wall effects and the mixing tee.

2. The transition line between wave and annular zones seems to be much closer to a horizontal line than to a vertical one as in previous maps.

3. There is a change of flow with length, and this seems to occur more frequently with a greater angle of inclination. It would be expedient to verify these findings with a larger length and other degrees of inclination.

4. Some flow regimes tend to disappear with increasing inclination. Examples are the plug flow going to bubble flow regime and stratified flow going to wavy flow regime.

5. The general trend of the pressure drop curves shows that for constant air flow rates the increase of water flow rates will increase the pressure drop relatively more at low air flow rates.

For constant water flow rates the results show that at low water flow rate values the pressure drop curves are very steep, while at high water flow rates they tend to be more horizontal.

6. Plug and slug flow regimes give large oscillations of pressure drop and these are even more pronounced with increased angles of inclination of the pipe.

7. There seems to be no sharp transition when one moves from one zone of the Baker map to another.

8. For constant water flow rates the oscillations are greater at low air flow rates.

9. In the slug flow regime the oscillations in the pressure drop at constant air flow rates decrease with increasing water flow rates.

10. In the slug flow regime a few negative pressure drops were recorded for some low flow rates of air due to the pulsations.

Recommendations

The general recommendations from this study are as follows:

1. Larger inclinations of the pipe should be studied.

2. A closed circuit for the water with a pump to provide sufficient flow rates of water should be employed, combined with an air compressor and pressure regulator to insure the same conditions at all times.

3. Sufficient pipe should be used to achieve fully developed flows and to observe clearly flow regime changes while eliminating effects of mixers, bends and outlets.

4. Special air-water mixers and inlet and outlet calming sections should be used to insure that pulsations are due only to the flow. This could also check the influence of external effects in the change of flow regimes with length.

5. The effects of changes in pressure and temperature on different gas-liquid combinations should be studied.

6. Pressure transducers connected to an oscillograph to measure pressure and record pulsations should be employed. Over a long period of time, this record could be used to correlate flow patterns with pressure pulsations.

7. Void fraction and its distribution should be measured. These parameters are an indirect measure of vapor liquid slip ratio and of film thickness. The film thickness can be used to evaluate heat transfer.

A SELECTED BIBLIOGRAPHY

(1) Alves, G. E. "Cocurrent-Liquid Gas Flow in a Pipe-Line Contactor." Chem. Eng. Prog., 50 (September, 1954), 449-456.

(2) Baker, O. "Designing for Simultaneous Flow of Oil and Gas." Oil and Gas J., 53 (July 26, 1954), 185-195.

(3) Hewitt, G. F., and H. Taylor. Annular Two-Phase Flow, 1st ed. Oxford: Pergamon Press, 1970.

(4) White, P. D., and R. L. Huntington. "Horizontal Co-Current Two-Phase Flow of Fluids in Pipe Lines." The Petroleum Engineer, 27 (August, 1955), D-40 - D-45.

(5) Govier, G. W., and M. M. Omer. "The Horizontal Pipeline Flow of Air-Water Mixtures." The Canadian J. of Chem. Eng., 40 (June, 1962), 93-104.

(6) Schicht, H. H. "Flow Patterns for an Adiabatic Two-Phase Flow of Water and Air Within a Horizontal Tube." Verfahrenstechnik, 3 (1969), 4, 153-161.

(7) Hoogendorn, C. J. "Gas-Liquid Flow in Horizontal Pipes." Chem. Eng. Sci., 9 (1959), 205-217.

(8) Krasiakova, C. L. "Some Characteristics of Two-Phase Flow Mixture in a Horizontal Pipe." Zhur. Tech. Fiz., 22, No. 4 (1952), 656.

(9) Bergelin, O. P., and C. Gazley, Jr. "Cocurrent Gas-Liquid Flow.I Flow in Horizontal Tubes." Proceedings, Heat Transfer and Fluid Mechanics Institute, June 22-24 (1949), Berkeley, California, ASME.

(10) Johnson, H. A., and A. H. Abou-Sabe. "Heat Transfer and Pressure Drop for Turbulent Flow of Air-Water Mixtures in a Horizontal Pipe." Trans. Am. Soc. Mech. Engrs., 74 (August, 1952), 977-987.

(11) Richardson, B. L. "Some Problems in Horizontal Two-Phase, Two-Component Flow." ANL-5949.

(12) Quandt, E. "Analysis of Gas-Liquid Flow Patterns." Chem. Eng. Prog. Symp., Series 61, No. 57 (1965), 128-135.

(13) Govier, G. W. "Developments in the Understanding of the Vertical Flow of Two Fluid Phases." The Canadian J. of Chem. Eng., 43 (February, 1965), 3-10.

(14) Kozlov, B. K. "Types of Gas-Liquid Mixtures and Stability Boundaries in Vertical Tubes." Zhur. Tech. Fiz., 24 (1952), 656.

(15) Galegar, W. C., W. B. Stovall, and R. L. Huntington. "Report on Two-Phase Vertical Flow." Pipeline Industry (February, 1956), 38-42.

(16) Griffith, P., and G. B. Wallis. "Two-Phase Slug Flow." A.S.M.E. Trans., Series C (August, 1961), pp. 307-370.

(17) Ros, N. C. J. "Simultaneous Flow of Gas and Liquid as Encountered in Well Tubing." J. Petrol. Technol. (1961), 1037-1049.

(18) Golan, L. P., and A. H. Stenning. "Two-Phase Vertical Flow Maps." Symposium, Fluid Mechanics and Measurements in Two-Phase Flow Systems, Paper No. 14. University of Leeds, September 24-25, 1969, p. 110.

(19) Bergles, A. E. "Electrical Probes for Study of Two-Phase Flows." Eleventh National ASME/ACHE Heat Transfer Conference, Minneapolis, Minnesota, August 3, 6, 1969, pp. 70-81.

(20) Lockhart, R. W., and R. C. Martinelli. "Proposed Correlation of Data for Isothermal Two-Phase, Two-Component Flow in Pipes." Chem. Eng. Prog., 45 (1949), 39-47.

(21) Martinelli, R. C., and D. B. Nelson. "Prediction of Pressure Drop During Forced-Circulation Boiling of Water." A.S.M.E. Trans., 70 (August, 1948), 695-702.

(22) Baker, O. "Multiphase Flow in Pipelines " Oil and Gas J., 57 (November 10, 1958), 156-165.

(23) Chenoweth, J. M., and M. W. Martin. "Turbulent Two-Phase Flow." Pet. Ref., 34 (October, 1955), 151-155.

(24) Brigham, W. E., E. D. Holstein, and R. L. Huntington. "How Uphill and Downhill Flow Affect Pressure Drop." Oil and Gas J., 45 (November 11, 1957), 145-152.

(25) Jacowitz, L. A., and R. S. Brodkey. "An Analysis of Geometry and Pressure Drop for the Horizontal, Annular, Two-Phase Flow of Water and Air in the Entrance Region of a Pipe." Chem. Eng. Sci., 19, No. 4 (April, 1964), 261-274.

(26) Dukler, A. E., M. Wicks, III, and R. G. Cleveland. "Frictional Pressure Drop in Two-Phase Flow; B. An Approach Through Similarity Analysis." Amer. Inst. Chem. Engr. J., 10 (January, 1964), 44-51.

(27) Bell, K. J. "Filmwise Condensation of Pure Components." (A personal communication)

APPENDIX A

NOMENCLATURE

A	annular flow regime
AN	mist flow regime
B	bubble flow regime
D	inside glass pipe diameter, in., ft
D_e	equivalent hydraulic diameter, in., ft
$\bar{d}$	density of a homogeneous mixture of liquid and gas, lb_m/ft^3
d_{eff}	effective density of a two-phase mixture, lb/ft^3
d_ℓ	density of liquid, lb_m/ft^3
$(dP/d\ell)$	local pressure gradient, psf/ft
d_v	density of gas, lb_m/ft^3
$\bar{F}r$	Froude number based on homogeneous gas-liquid mixture, $[-]$
f	Fanning friction factor of single phase, $[-]$
f_{TP}	friction factor of two-phase mixture, $[-]$
G	superficial mass velocity of the mixture, $lb_m/hr\text{-}ft^2$
G_ℓ	superficial mass velocity of the liquid, $lb_m/hr\text{-}ft^2$
G_v	superficial mass velocity of the gas, $lb_m/hr\text{-}ft$
g	local acceleration of gravity, ft/hr^2
g_c	gravitational conversion constant, $4.17*10^8$ $lb_m\text{-}ft/lb_f\text{-}hr^2$
h	height of water in the manometer, in.
L	length of glass pipe, ft
L′	superficial mass velocity of the liquid, $lb_m/hr\text{-}ft^2$
M_ℓ*	liquid mass flow rate, kg/sec
M_G*	gas mass flow rate, kg/sec
P	plug flow regime
P′	system static pressure, lb_f/ft^2

P_c	critical pressure of gas, lb_f/ft^2
P_r	reduced pressure of gas, [-]
$(Re)_{\ell \text{ or } v}$	Reynolds numbers of the liquid and gas phases, respectively, [-]
R_ℓ	liquid volume fraction, [-]
R_v	gas phase volume fraction, [-]
S	cross-sectional area of conduit, ft^2, $in.^2$
SL	slug flow regime
ST	stratified flow regime
s	slip ratio, [-]
V_ℓ	liquid volume flow rate, gal/min
V_v	gas volume flow rate, ft^3/min
$\bar{v}$	linear velocity of homogeneous gas-liquid mixture, ft/sec; ft/hr
v_ℓ, v_v	true mean velocities of the liquid and gas phases, respectively, ft/hr; ft/sec
W	wavy flow regime
W_e	Weber number based on homogeneous liquid velocity and density, [-]
W_ℓ	liquid mass flow rate, lb_m/min; lb_m/hr
W_v	gas mass flow rate, lb_m/min; lb_m/hr
X	flow weight quality of mixture, [-]
x	abscissa of transformed Baker map, $\frac{lb^{2/3}\text{-cm}}{hr^{4/3}\text{-}ft^{1/3}\text{-dyne}}$
y	ordinate of transformed Baker map, ft/hr
α	angle of orientation to vertical
Γ	minimum flow rate for a continuous liquid film

Δh	manometer indication, in.
ΔP	pressure drop, psf/ft
$(\Delta P/\Delta L)_f$	pressure drop due to friction, psf/ft
$(\Delta P/\Delta L)_g$	pressure drop due to hydrostatic effects, psf/ft
$(\Delta P/\Delta L)_M$	experimentally measured pressure drop, psf/ft
Λ	Baker flow regime parameter, $\Lambda = \sqrt{d_v d_\ell}$ lb_m/ft^3
λ	parameters used by Baker in the original version of his flow regime map, $\left[-\right]$
$\overline{\mu}$	viscosity of homogeneous mixture, lb/ft-hr
μ_L	viscosity of liquid, lb_m/ft-hr
μ_v	viscosity of gas, lb_m/ft-hr
σ	surface tension, dyne/cm
ϕ	Lockhart-Martinelli two-phase pressure drop parameter, $\left[-\right]$
χ_{tt}	Martinelli parameter for two-phase flow, $\left[-\right]$
ψ	Baker flow regime map parameter; $cm\text{-}ft^{\frac{5}{6}}/dyne\text{-}hr^{\frac{1}{3}}\text{-}lb_m^{\frac{1}{3}}$
$\overline{\psi}$	$centipoise^{\frac{2}{3}}$

APPENDIX B

PHOTOGRAPHS OF CHARACTERISTIC FLOW PATTERNS

Figure 17. Horizontal Pipe, Plug Flow

$G_\ell \psi = 2.9 \times 10^2$

$G_v / \Lambda = 5.3 \times 10^2$

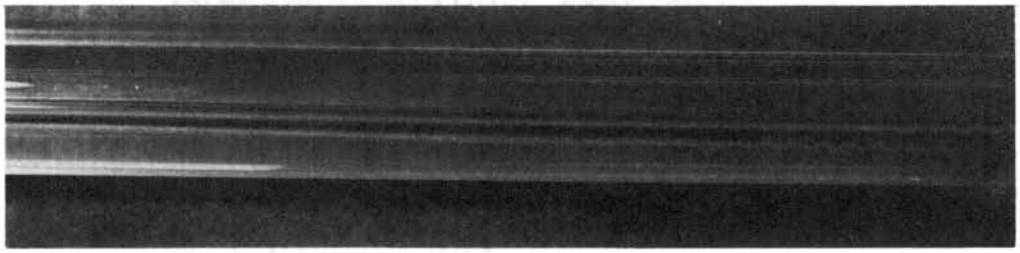

Figure 18. Horizontal Pipe, Stratified Flow

$G_\ell \psi = 3.7 \times 10^1$

$G_v / \Lambda = 2.5 \times 10^2$

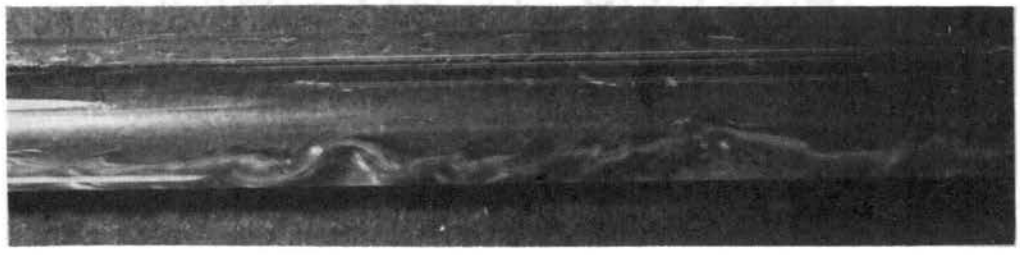

Figure 19. Horizontal Pipe, Wavy Flow

$G_\ell \psi = 3.9 \times 10^1$

$G_v / \Lambda = 3.5 \times 10^3$

Figure 20. Horizontal Pipe, Annular Flow

$G_\ell \psi = 4.9 \times 10^2$

$G_v / \Lambda = 8.0 \times 10^3$

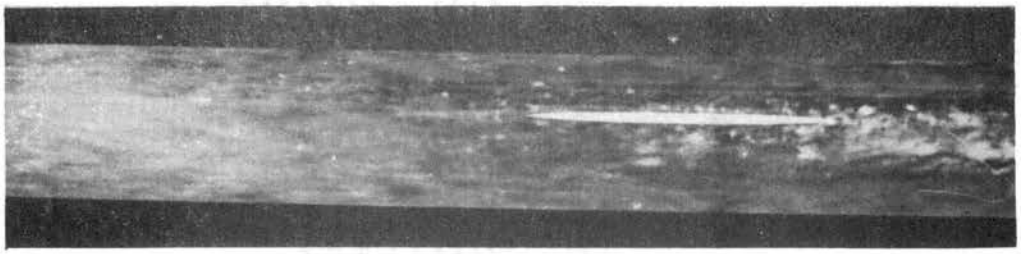

Figure 21. Horizontal Pipe, Slug Flow

$G_\ell \psi = 5.2 \times 10^2$

$G_v / \Lambda = 1.8 \times 10^3$

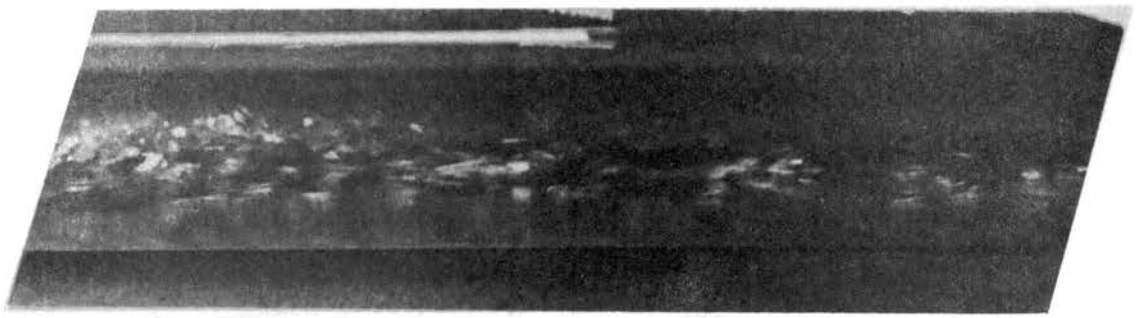

Figure 22. Pipe Inclined 15°, Bubble Flow

$G_\ell \psi = 4.1 \times 10^2$

$G_v / \Lambda = 5.6 \times 10^2$

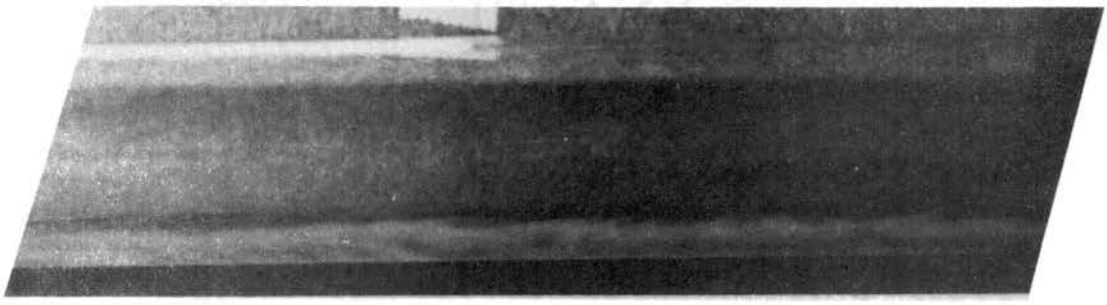

Figure 23. Pipe Inclined 15°, Stratified Flow

$G_\ell \psi = 1.9 \times 10^1$

$G_v / \Lambda = 8.1 \times 10^2$

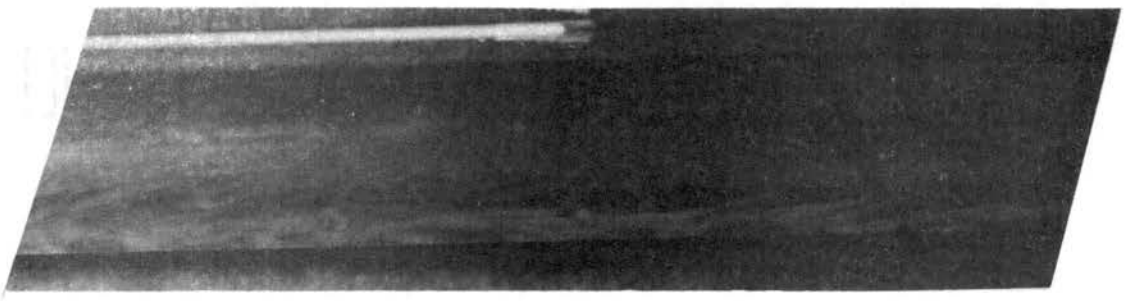

Figure 24. Pipe Inclined 15°, Wavy Flow

$G_\ell \psi = 3.5 \times 10^1$

$G_v / \Lambda = 5.0 \times 10^3$

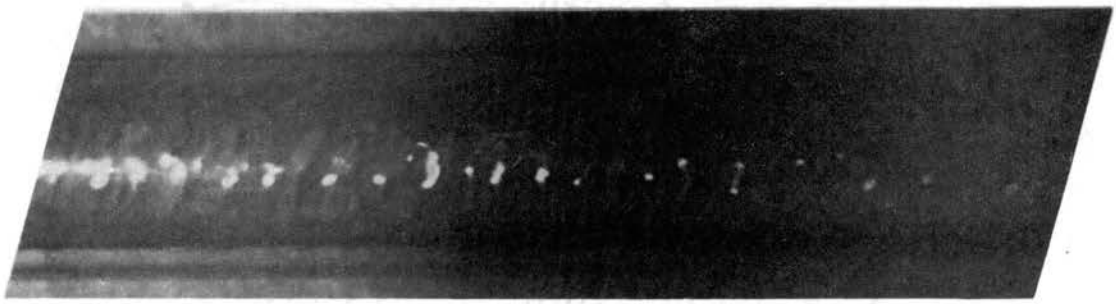

Figure 25. Pipe Inclined 15°, Annular Flow

$G_\ell \psi = 3.5 \times 10^2$

$G_v / \Lambda = 8.2 \times 10^3$

Figure 26. Pipe Inclined 15°, Slug Flow

$G_\ell \psi = 2.1 \times 10^2$

$G_v / \Lambda = 3.9 \times 10^3$

APPENDIX C

PRESSURE DROP CONTRIBUTIONS

The friction and hydrostatic contribution to the pressure drop in the experiment can be estimated using the following equation:(27):

$$\left(\frac{\Delta P}{\Delta L}\right)_M = \left(\frac{\Delta P}{\Delta L}\right)_f + \left(\frac{\Delta P}{\Delta L}\right)_g = \left(\frac{\Delta P}{\Delta L}\right)_f + \frac{g}{g_c}\ \rho_{eff}\ \cos\alpha \qquad (C.1)$$

To evaluate these terms we need to define

$$x = \frac{W_v}{W_v + W_\ell} \qquad (C.2)$$

$$G_v = \frac{W_v}{S} \qquad (C.3)$$

$$G_\ell = \frac{W_\ell}{S} \qquad (C.4)$$

$$\rho_{eff} = R_v d_v + R_\ell d_\ell \qquad (C.5)$$

$$X_{tt} = \left(\frac{1-x}{x}\right)\left(\frac{d_v}{d_\ell}\right)^{0.57}\left(\frac{\mu_\ell}{\mu_v}\right)^{0.11} \qquad (C.6)$$

$$P_r = \frac{P'}{P_c} \text{ of the air} \qquad (C.7)$$

Then if

$$(R_e)_\ell = \frac{D G_\ell}{\mu_\ell} > 2100 \qquad (C.8)$$

we can use

$$f_\ell = \frac{0.078}{\left(\frac{D G_\ell}{\mu_\ell}\right)^{\frac{1}{4}}} \qquad (C.9)$$

and

$$\left(\frac{dP}{d\ell}\right)_{f,\ell} = \frac{-2 f_\ell G_\ell^2}{g_c d_\ell D} \qquad (C.10)$$

and

$$\left(\frac{\Delta P}{\Delta L}\right)_f = \Phi^2_{tt} \left(\frac{dP}{d\ell}\right)_{f,\ell} \tag{C.11}$$

But if

$$(Re)_\ell < 2100$$

and

$$(Re)_v = \left(\frac{DG_v}{\mu_v}\right) > 2100 \tag{C.12}$$

we will use

$$f_v = \frac{0.078}{\left[\frac{DG_v}{\mu_v}\right]^{\frac{1}{4}}} \tag{C.13}$$

and

$$\left(\frac{dP}{d\ell}\right)_{f,v} = -\frac{2 f_v G_v^2}{g_c d_v D} \tag{C.14}$$

with

$$\left(\frac{\Delta P}{\Delta L}\right)_f = \Phi^2_{tt} \chi^{1.75} \left(\frac{dP}{d\ell}\right)_{f,v} \tag{C.15}$$

If both $(Re)_\ell$ and $(Re)_v < 2100$, we should use the Fanning function chart, but probably the pressure drop will be negligible.

R_ℓ, R_v and Φ_{tt} are found with the Martinelli-Nelson correlations as functions of $\sqrt{\chi_{tt}}$ and P_r.

It is now possible to tabulate the results for three extreme cases for the 15° inclination pipe:

$$\left(\frac{d_v}{d_\ell}\right)^{0.57} = \left(\frac{0.0807}{62.3}\right)^{0.57} = 0.024 \tag{C.16}$$

$$\left(\frac{\mu_\ell}{\mu_v}\right)^{0.11} = \left(\frac{1.0019}{0.01815}\right) = 1.55 \qquad \text{(C.17)}$$

$$P_c = 545 \text{ psia}$$

$$P_r = 0.029$$

$$W_\ell = V_\ell \text{ gal/min} * 8.34 \text{ lb/gal} * 60 \text{ min/hr} = 500\ V_\ell \text{ lb/hr}$$

$$W_v = V_v \text{ ft}^3\text{/min} * 0.0807 \text{ lb/ft}^3 * 60 \text{ min/hr} = 4.85\ V_v \text{ lb/hr.}$$

We can conclude from the following table that the contribution of the hydrostatic effect to the total pressure drop will be from 10 to 65 percent in the extreme cases while in a normal case it will be approximately 40 percent.

TABLE I

PRESSURE DROP ESTIMATIONS

First Calculation	Second Calculation	Third Calculation	Parameters
1	20	10	V_v
8	0.1	1	V_ℓ
0.00121	0.66	0.0885	x
824	0.515	10.4	$\frac{1-x}{x}$
5.6	0.138	0.62	$\sqrt{X_{tt}}$
0.7	0.018	0.14	R_ℓ
0.3	0.982	0.86	R_v
43.6	1.12	8.7	$R_\ell d_\ell$
0.0024	0.08	0.07	$R_v d_v$
732,000	17,700	91,500	G_ℓ or G_v
0.0062	0.0058	0.0104	f_ℓ or f_v
1.5	42	6.6	Φ_{tt}
11.3	0.31	2.28	$\left(\frac{\Delta P}{\Delta L}\right)_g$
2.89	1.29	$8 * 10^{-2}$	$\left(\frac{dP}{d\ell}\right)_{f,\ell \text{ or } v}$
6.5	2.28	3.50	$\left(\frac{\Delta P}{\Delta L}\right)_f$
17.8	2.59	5.78	$\left(\frac{\Delta P}{\Delta L}\right)_M$
0.635	0.12	0.395	$\frac{(\Delta P/\Delta L)_g}{(\Delta P/\Delta L)_M}$

APPENDIX D

EXPERIMENTAL AND CALCULATED DATA

Nomenclature

A	annular flow regime
B	bubble flow regime
P	plug flow regime
SL	slug flow regime
ST	stratified flow regime
V_ℓ	liquid volume flow rate, gal/min
V_v	gas volume flow rate, ft^3/min
W	wavy flow regime
Δh_{av}	average manometer indication, in. of water
Δh_{ma}	maximum manometer indication, in. of water
Δh_{mi}	minimum manometer indication, in. of water
ΔP_{ave}	average pressure drop, psf/ft length
ΔP_{ma}	maximum pressure drop, psf/ft length
ΔP_{mi}	minimum pressure drop, psf/ft length
λ	Baker flow regime parameter, lb_m/ft^3
ψ	Baker flow regime parameter, $\frac{\text{cm-ft}^{5/3}}{\text{dyn-hr}^{\frac{1}{3}}\text{-lb}_m^{\frac{1}{3}}}$

The ordinates of the Baker map were calculated using Equation (5.4) where $y = G_v/\lambda$ represents the ordinate.

The abscissas of the Baker map were calculated using Equation (5.5) where $x = G_\ell\psi$ represents the abscissa.

The pressure drops were calculated using Equation (5.1) in which

1. $h_1 - h_2 = 0.0$ in the horizontal case;
2. $h_1 - h_2 = 10 * 12 * \sin 5^\circ$ for the pipe inclined 5°;
3. $h_1 - h_2 = 10 * 12 * \sin 15^\circ$ for the pipe inclined 15°.

Sample Calculation

For run No. 78 in the case of pipe inclined 15°

$$\Delta h_{ave} = 37$$

$$\Delta h_{max} = 39$$

$$\Delta h_{min} = 36$$

$$V_{\ell} = 1.825$$

$$V_{v} = 15.257$$

$$y = G_{v}/\Lambda = \frac{V_{v}}{2.5228 * 10^{-3}} = \frac{15.257}{2.5228 * 10^{-3}} = 6.047 * 10^{3}$$

$$x = G_{\ell}\psi = \frac{V_{\ell}}{9.304 * 10^{-3}} = \frac{1.825}{9.304 * 10^{-3}} = 1.96 * 10^{2}$$

$$\Delta P_{ave} = \frac{1}{10}\left[\frac{37}{12}(62.3 - 0.08) - \frac{62.3}{12}(10 * 12 * \sin 15^{\circ})\right] = 2.984$$

$$\Delta P_{max} = \frac{1}{10}\left[\frac{39}{12}(62.3 - 0.08) - \frac{62.3}{12}(10 * 12 * \sin 15^{\circ})\right] = 4.021$$

$$\Delta P_{min} = \frac{1}{10}\left[\frac{36}{12}(62.3 - 0.08) - \frac{62.3}{12}(10 * 12 * \sin 15^{\circ})\right] = 2.466$$

The Flow column refers to the possible visual observation of the flow regime which in some cases corresponds to two or three different possible flows because it was difficult to distinguish which one was the true flow regime.

The runs in the tables which are indicated by arrows (→) designate changes of flow pattern with length of pipe.

TABLE II

EXPERIMENTAL AND CALCULATED DATA IN HORIZONTAL PIPE

Run	V_v	Δh_{max}	Δh_{min}	Δh_{ave}	Flow	G_v/Λ	ΔP_{max}	ΔP_{min}	ΔP_{ave}
Series No. 1. V_ℓ = 1.561						Series No. 1. $G_\ell\psi$ = 1.7 * 10^2			
1	1.045	7	-1	2	P-ST-W	4.142 * 10^2	3.629	-0.518	1.036
2	2.090	8	-1	2.5	SL-W-P	8.284 * 10^2	4.147	-0.518	1.296
3	3.135	8	-1	2.5	SL-W-P	1.242 * 10^3	4.147	-0.518	1.296
4	4.075	8	-1	2.5	SL-W	1.615 * 10^3	4.147	-0.518	1.296
5	5.225	8	0.5	3.0	SL	2.071 * 10^3	4.147	0.259	1.549
6	6.270	7	0.5	3.5	SL	2.485 * 10^3	3.629	0.259	1.814
7	7.524	6.5	3	4.0	SL	2.982 * 10^3	3.370	1.555	2.075
8	10.030	7	4	5.5	SL-A	3.975 * 10^3	3.629	2.074	2.851
9	20.480	21	18	20	A	8.117 * 10^3	10.888	9.332	10.369
10	14.212	11	8.5	10	A	5.633 * 10^3	5.703	4.407	5.184
11	11.495			7	SL-A	4.556 * 10^3			3.629
12	12.540	10	7	9	A	4.970 * 10^3	5.184	3.629	4.666
Series No. 2. V_ℓ = 0.335						Series No. 2. $G_\ell\psi$ = 3.6 * 10^1			
13	10.241	2.1	1.9	2	W	4.059 * 10^3	1.088	0.985	1.036
14	4.598	0.5	0.35	0.45	ST-W	1.822 * 10^3	0.259	0.181	0.233
15	3.553			0.35	ST	1.408 * 10^3			0.181
16	2.508			0.3	ST	9.941 * 10^2			0.155
17	5.225			0.45	W-ST	2.071 * 10^3			0.233
18	7.106	0.95	0.65	0.8	W	2.816 * 10^3	0.492	0.337	0.414
19	8.882	1.3		1.2	W	3.520 * 10^3	0.674		0.622
20	12.540		2.3	2.7	W-A	4.970 * 10^3		1.192	1.399
21	15.466			4	A-W	6.130 * 10^3			2.073
22	17.347			5	A	6.876 * 10^3			2.592
23	18.392			5.5	A	7.290 * 10^3			2.851
24	20.480			7	A	8.117 * 10^3			3.629
Series No. 3. V_ℓ = 0.190						Series No. 3. $G_\ell\psi$ = 2.05 * 10^1			
25	18.392			4.5	A	7.290 * 10^3			2.333
26	12.958	2.6	2	2.1	W	5.136 * 10^3	1.348	1.036	1.088
27	15.257			2.7	W-A	6.047 * 10^3			1.399
28	14.421			2.5	W-A	5.716 * 10^3			1.296
29	15.466			2.8	A-W	6.130 * 10^3			1.451
30	16.511			3.4	A	6.544 * 10^3			1.762
31	20.064			5	A	7.952 * 10^3			2.592
32	5.852	0.5		0.45	ST	2.139 * 10^3			0.233
33	6.897			0.55	ST	2.733 * 10^3			0.285
34	8.673	0.9	0.75	0.8	W-ST	3.438 * 10^3	0.466	0.388	0.414
35	9.823			1.1	W-ST	3.893 * 10^3			0.570
36	10.450			1.25	W	4.142 * 10^3			0.648
37	11.495			1.65	W	4.556 * 10^3			0.855

TABLE II (Continued)

Run	V_v	Δh_{max}	Δh_{min}	Δh_{ave}	Flow	G_v/Λ	ΔP_{max}	ΔP_{min}	ΔP_{ave}
Series No. 4. V_ℓ = 0.220						Series No. 4. $G_\ell\psi$ = 2.36 * 10^1			
38	13.585	2.5		2.4	W-A	5.384 * 10^3	1.296		1.244
39	5.956			0.5	ST	2.361 * 10^3			0.259
40	4.180			0.3	ST	1.656 * 10^3			0.155
41	8.151	0.9	0.75	0.8	ST-W	3.230 * 10^3	0.466	0.388	0.414
42	8.987		0.85	0.9	ST-W	3.562 * 10^3		0.440	0.466
43	9.405			1.1	W	3.727 * 10^3			0.570
44	10.241			1.3	W	4.059 * 10^3			0.674
45	10.659			1.45	W	4.225 * 10^3			6.751
46	11.077			1.6	W	4.390 * 10^3			0.829
47	12.331			2.0	W-A	4.887 * 10^3			1.036
48	12.853			2.25	W-A	5.094 * 10^3			1.166
49	14.421			2.85	W-A	5.716 * 10^3			1.477
50	15.884			3.4	A-W	6.296 * 10^3			1.762
51	17.347			4.5	A	6.876 * 10^3			2.333
52	19.855		5.1	5.5	A	7.870 * 10^3		2.644	2.851
Series No. 5. V_ℓ = 0.115						Series No. 5. $G_\ell\psi$ = 1.24 * 10^1			
53	18.601			3.5	A	7.373 * 10^3			1.814
54	12.122			1.4	W-ST	4.804 * 10^3			0.725
55	7.315			0.6	ST	2.899 * 10^3			0.311
56	6.270			0.5	ST	2.485 * 10^3			0.259
57	8.360			0.7	ST	3.313 * 10^3			0.362
58	9.614			0.8	ST-W	3.810 * 10^3			0.414
59	10.450			0.9	ST-W	4.142 * 10^3			0.466
60	11.495			1.25	W-ST	4.556 * 10^3			0.648
61	12.540			1.65	W	4.970 * 10^3			0.855
62	13.585			1.90	W	5.384 * 10^3			0.985
63	15.884			2.55	W-A	6.296 * 10^3			1.322
64	16.929			3	A	6.710 * 10^3			1.555
65	20.273			3.9	A	8.035 * 10^3			2.022
Series No. 6. V_ℓ = 7.986						Series No. 6. $G_\ell\psi$ = 8.58 * 10^2			
66	0.731			11	P	2.899 * 10^2			5.703
67	1.358		14	14.5	P	5.384 * 10^2		7.258	7.518
68	1.985			18	SL-P	7.870 * 10^2			9.332
69	3.418	26	21	23	SL	1.366 * 10^3	13.480	10.888	11.925
70	6.688	40		36	SL	2.651 * 10^3	20.739		18.665
71	7.375	44		40	SL	2.899 * 10^3	22.813		20.739
72	8.882	50		45	SL	3.520 * 10^3	25.924		23.331
73	10.450	55		52	SL-A	4.142 * 10^3	28.516		26.961
74	0.836			11.5	P	3.313 * 10^2			5.962
75	1.149			13	P	4.556 * 10^2			6.740

TABLE II (Continued)

Run	V_v	Δh_{max}	Δh_{min}	Δh_{ave}	Flow	G_v/Λ	ΔP_{max}	ΔP_{min}	ΔP_{ave}
76	1.672			16.5	P	$6.627 * 10^2$			8.555
77	2.403	22	16	19	SL-P	$9.526 * 10^2$	11.406	8.295	9.851
78	3.030			21	SL	$1.201 * 10^3$			10.888
Series No. 7. V_ℓ = 3.348						Series No. 7. $G_\ell\psi = 3.65 * 10^2$			
79	1.149	5.5	4	4.6	P	$4.556 * 10^2$	2.851	2.073	2.385
80	1.985	8.5	7	6.5	P-SL	$7.870 * 10^2$	4.407	3.629	3.370
81	3.657	13	3	7	SL	$1.449 * 10^3$	6.740	1.555	3.629
82	4.702	15	5	8	SL	$1.863 * 10^2$	7.777	2.592	4.147
83	7.524	18	8	10	SL	$2.982 * 10^3$	9.332	4.147	5.184
84	10.450	23	16	19	SL-A	$4.142 * 10^3$	11.925	8.295	9.851
85	12.540	23	17	20	A-SL	$4.970 * 10^3$	11.925	8.814	10.369
86	14.630	28	20	24	A-SL	$5.799 * 10^3$	14.517	10.369	12.443
87	16.720	31	23	28	A	$6.627 * 10^3$	16.073	11.925	14.517
88	18.601	34	30	32	A	$7.373 * 10^3$	12.628	15.554	16.591
89	20.064	38	32	35	A	$7.952 * 10^3$	19.702	16.591	18.147
Series No. 8. V_ℓ = 0.840						Series No. 8. $G_\ell\psi = 9.0 * 10^1$			
90	7.315	2.8	0.6	1.5	W-SL-ST	$2.899 * 10^3$	1.451	0.311	0.777
91	2.090	10	-1.5	0.5	ST-SL-W	$8.284 * 10^2$	5.184	-0.777	0.259
92	1.045	5	-1	0.4	ST-P-W	$4.142 * 10^2$	2.592	-0.518	0.207
93	9.405	3		3.2	W-SL-A	$3.727 * 10^3$	1.555		1.659
94	4.493	3	0	1.1	ST-SL	$1.781 * 10^3$	11		0.570
95	12.122	4.1	3.5	3.9	W-A	$4.804 * 10^3$	2.125	1.814	2.022
96	17.138	8.6	8.4	8.5	A	$6.793 * 10^3$	4.458	4.355	4.407
97	14.630			6	A	$5.799 * 10^2$			3.110
98	10.450			3.5	W-A-SL	$4.142 * 10^3$			1.814
99	8.360	2.5	2	2.1	W-SL-ST	$3.313 * 10^3$	1.296	1.036	1.088
100	9.405			2.5	W	$3.727 * 10^3$			1.296
101	20.900			13	A	$8.284 * 10^3$			6.740
Series No. 9. V_ℓ = 0.040						Series No. 9. $G_\ell\psi = 4.35 * 10^0$			
102	13.601			2.7	A-W	$7.373 * 10^3$			1.399
103	14.421			1.3	ST-W	$5.716 * 10^3$			0.674
104	15.048			1.65	W-ST	$5.964 * 10^3$			0.855
105	16.197			1.9	W	$6.420 * 10^3$			0.985
106	20.900			3.3	W-A	$8.284 * 10^3$			1.710

TABLE III

EXPERIMENTAL AND CALCULATED DATA IN PIPE INCLINED 5°

Run	V_v	Δh_{max}	Δh_{min}	Δh_{ave}	Flow	G_v/Λ	ΔP_{max}	ΔP_{min}	ΔP_{ave}
Series No. 1. V_ℓ = 4.761						Series No. 1. $G_\ell\psi = 5.2 * 10^2$			
1	0.836	11	10.55	10.65	P-W	$3.313 * 10^2$	0.303	0.070	0.122
2	2.090	18	11.5	14.5	SL	$8.284 * 10^2$	3.93	1.859	0.567
3	4.180	28	20	23	SL	$1.656 * 10^3$	9.118	1.340	4.970
4	5.434	30	17	21	SL	$2.153 * 10^3$	10.155	3.414	5.488
5	7.524	33	20	24	SL-A	$2.982 * 10^3$	11.710	1.340	7.044
6	12.331	58	30	34	SL-A	$4.887 * 10^3$	24.673	10.155	12.229
7	15.675	53	41	45	A-SL	$6.213 * 10^3$	22.080	16.377	17.932
8	17.974	50	50	53	A-SL	$7.124 * 10^3$	25.71	20.525	22.080
9	19.855			60	A-SL	$7.870 * 10^3$			25.710
10	0.418	10.9	10.5	10.60	W	$1.656 * 10^3$	0.251	0.044	0.096
Series No. 2. V_ℓ = 1.175						Series No. 2. $G_\ell\psi = 1.28 * 10^2$			
11	0.940			10.5	ST-W-P	$3.729 * 10^2$			0.044
12	0.522			10.5	ST	$2.071 * 10^2$			0.044
13	2.195	10.7		10.5	W-ST-SL	$8.698 * 10^2$	0.147		0.044
14	4.180	10.9	10.5	10.7	W-ST	$1.656 * 10^3$	0.251	0.044	0.147
15	6.270	11.4	11	11.3	W	$2.485 * 10^3$	0.510	0.303	0.459
16	8.360	12.5	11.5	12	W	$3.313 * 10^3$	1.081	0.562	0.822
17	10.241	15		14	W-A-SL	$4.059 * 10^3$	2.377		1.859
18	12.540	15.5		15	A-W	$4.970 * 10^3$	2.636		2.375
19	14.421	17.5	16	16.5	A-W-SL	$5.716 * 10^3$	3.673	2.896	3.155
20	19.855			24	A	$7.870 * 10^3$			7.044
21	16.720			20	A	$6.627 * 10^3$			4.970
22	15.884	19	18	18.5	A	$6.296 * 10^3$	4.451	3.933	4.192
23	12.958	16.5	15.5	16	A-W	$5.136 * 10^3$	3.155	2.436	2.896
Series No. 3. V_ℓ = 0.071						Series No. 3. $G_\ell\psi = 7.8 * 10^0$			
24	5.852			10.7	ST	$2.319 * 10^3$			0.147
25	8.882			11.1	ST	$3.520 * 10^3$			0.355
26	10.032			11.2	ST	$3.976 * 10^3$			0.407
27	13.585			11.6	ST	$5.384 * 10^3$			0.614
28	17.556			13	W	$6.958 * 10^3$			1.340
29	20.482			14.1	A-W	$8.118 * 10^3$			1.910
30	14.630			11.9	W-ST	$5.799 * 10^3$			7.701
31	16.720			12.4	W	$6.627 * 10^3$			1.029
32	18.810			13.5	A-W	$7.455 * 10^3$			1.651
33	20.900			14.3	A-W	$8.284 * 10^3$			2.014
Series No. 4. V_ℓ = 1.575						Series No. 4. $G_\ell\psi = 1.72 * 10^2$			
34	6.061	11.5	10.5	11	W-SL	$2.402 * 10^3$	0.562	0.044	0.303
35	1.149	11.2	10.5	10.8	W	$4.556 * 10^2$	0.407	0.044	0.199

TABLE III (Continued)

Run	V_v	Δh_{max}	Δh_{min}	Δh_{ave}	Flow	G_v/Λ	ΔP_{max}	ΔP_{min}	ΔP_{ave}
36	0.522			10.6	W-ST	$2.071 * 10^2$			0.096
37	9.196	13.5	12.5	13	A-W-SL	$3.645 * 10^2$	1.599	1.081	1.340
38	6.688	11.8	10	11.1	W-SL	$2.650 * 10^3$	0.718	-0.215	0.355
39	7.733	13	11	12.2	W-SL	$3.065 * 10^3$	1.340	0.303	0.925
40	11.704	18		16	A-SL	$4.639 * 10^3$	3.933		2.896
41	12.540			16.8	A	$4.970 * 10^3$			3.310
42	14.630	21		19	A	$5.799 * 10^3$	5.488		4.451
43	16.72	24		23	A	$6.627 * 10^3$	7.044		6.525
44	18.81	27	26	26.5	A	$7.455 * 10^3$	8.599	8.018	8.340
45	20.90	31		30	A	$8.284 * 10^3$	10.673		10.155
Series No. 5. $V_\ell = 0.192$						Series No. 5. $G_\ell\psi = 2.1 * 10^1$			
46	7.315			11	ST-W	$2.895 * 10^3$			0.303
47	7.942			11.1	ST-W	$3.148 * 10^3$			0.355
48	9.614			11.25	W-ST	$3.810 * 10^3$			0.433
49	10.868			11.4	W-ST	$4.307 * 10^3$			0.510
50	11.390			11.5	W-ST	$4.516 * 10^3$			0.562
51	12.853			12	W-SL	$5.094 * 10^3$			0.822
52	13.794			12.5	SL-W	$5.467 * 10^3$			1.081
53	16.720			13.4	A-W-SL	$6.627 * 10^3$			1.547
54	17.138			14	A-SL	$6.793 * 10^3$			1.859
55	19.332			15	A	$7.663 * 10^3$			2.377
56	20.900			15.9	A	$8.284 * 10^3$			2.844
Series No. 6. $V_\ell = 7.38$						Series No. 6. $G_\ell\psi = 7.93 * 10^2$			
57	0.836	12.5	11.5	11.8	P	$3.313 * 10^2$	1.081	0.562	7.183
58	1.254	19	14	16	P	$4.970 * 10^2$	4.451	1.359	2.896
59	1.881	21	16	20	P-SL	$7.455 * 10^2$	5.488	2.896	4.970
60	3.135	30	21	25	SL	$1.242 * 10^3$	10.155	5.488	7.562
61	5.225	40	22	30	SL	$2.071 * 10^3$	15.340	6.007	10.155
62	8.360	50	34	42	SL-A	$3.313 * 10^3$	20.525	12.229	16.377
63	10.450			50	SL-A	$4.140 * 10^3$			20.525
64	14.421			60	SL-A	$5.716 * 10^3$			25.710
65	13.376			55	SL-A	$5.301 * 10^3$			23.117
Series No. 7. $V_\ell = 2.021$						Series No. 7. $G_\ell\psi = 2.2 * 10^2$			
66	4.180	11.5	9	11	W-SL	$1.656 * 10^3$	0.562	-0.733	0.303
67	5.225	12	10	11.2	W-SL	$2.071 * 10^3$	0.822	-0.215	0.407
68	8.360	15	11	13.5	SL-W-A	$3.313 * 10^3$	2.375	0.303	1.599
69	14.421	22	19	21	A-SL	$5.716 * 10^3$	6.007	4.451	5.488
70	15.675	25	20	22	A-SL	$6.213 * 10^3$	7.562	4.970	6.007
71	18.810	31	29.5	30.5	A	$7.455 * 10^3$	10.673	9.895	10.414
72	20.900			35	A	$8.284 * 10^3$			12.747

TABLE III (Continued)

Run	V_v	Δh_{max}	Δh_{min}	Δh_{ave}	Flow	G_v/A	ΔP_{max}	ΔP_{min}	ΔP_{ave}
73	0.627			10.8	W	$2.485 * 10^2$			0.199
74	1.045			10.6	W	$4.142 * 10^2$			0.096
75	3.135			11	W	$1.242 * 10^3$			0.303
Series No. 8. $V_\ell = 0.707$						Series No. 8. $G_\ell\psi = 7.7 * 10^1$			
76	4.180			10.8	W-ST	$1.656 * 10^3$			0.199
77	7.524			11.1	W	$2.982 * 10^3$			0.355
78	11.703	14	13	13.5	→A-W-SL	$4.639 * 10^3$	1.859	1.340	1.599
79	14.630	15.2	14.6	15	→A-SL	$5.795 * 10^3$	2.481	2.170	2.375
80	17.242			17	→A-SL	$6.834 * 10^3$			3.414
81	19.850	20		19.5	A	$2.868 * 10^3$	4.970		4.710
82	20.900			21	A	$8.284 * 10^3$			5.488
83	14.212			14.5	A-SL	$5.633 * 10^3$			2.118
84	10.450	13.2	12	12.5	→A-W-SL	$4.142 * 10^3$	1.444	0.822	1.081
85	8.778			11.5	W	$3.479 * 10^3$			0.562
86	6.688			11	W	$2.650 * 10^3$			0.303
87	3.135			10.7	→W-ST	$1.242 * 10^3$			0.147
88	1.254			10.6	→W-ST	$4.970 * 10^2$			0.096
Series No. 9. $V_\ell = 0.431$						Series No. 9. $G_\ell\psi = 4.7 * 10^1$			
89	3.762	10.9	10.4	10.6	→W-ST	$1.491 * 10^3$	0.251	-0.007	0.096
90	1.672			10.6	ST	$6.627 * 10^2$			0.056
91	5.434			10.9	→W-ST	$2.953 * 10^3$			0.251
92	2.733			11.15	W	$3.065 * 10^3$			0.381
93	9.196	11.5		11.35	W	$3.645 * 10^3$	0.562		0.484
94	10.241	11.6		11.5	W	$4.059 * 10^3$	0.614		0.562
95	11.704			12	→W-SL	$4.639 * 10^3$			0.822
96	14.421			14	A-W	$5.716 * 10^3$			1.859
97	15.675			14.4	A	$6.213 * 10^3$			2.066
98	18.392			16.3	A	$7.290 * 10^3$			3.051
99	20.900			18.4	A	$8.284 * 10^3$			4.140
100	13.167			13.5	A-W-SL	$5.219 * 10^3$			1.599
Series No. 10. $V_\ell = 4.125$						Series No. 10. $G_\ell\psi = 4.5 * 10^2$			
101	2.090	10.5	11.5	11.1	W-SL	$8.284 * 10^2$	0.562	0.044	0.355
102	0.836			10.6	W	$3.313 * 10^2$			0.096
103	1.672			10.7	W	$6.627 * 10^2$			0.147
104	3.344	18	10	13	SL-W	$1.325 * 10^3$	3.933	-0.215	1.340
105	5.225	21	10	15	SL	$2.071 * 10^3$	5.488	-0.215	2.375
106	8.360	28	14	18	SL	$3.313 * 10^3$	9.118	1.859	3.933
107	10.868	35	23	26	SL-A	$4.307 * 10^3$	12.747	6.525	8.081
108	13.754	35	26	30	→A-SL	$5.467 * 10^3$	12.747	8.081	10.155
109	16.720	45		39	→A-SL	$6.627 * 10^3$	17.932		14.821

TABLE III (Continued)

Run	V_v	Δh_{max}	Δh_{min}	Δh_{ave}	Flow	G_v/Λ	ΔP_{max}	ΔP_{min}	ΔP_{ave}
Series No. 11. $V_\ell = 7.961$						Series No. 11. $G_\ell\Psi = 8.7 * 10^2$			
110	1.045			12.5	P	$4.142 * 10^2$			1.081
111	2.090			16.5	-P-B	$8.284 * 10^2$			3.155
112	3.135	28	23	24	SL	$1.242 * 10^3$	9.118	6.525	7.044
113	4.980	35	25	29	SL	$1.822 * 10^3$	12.747	7.562	9.636
114	6.270	38	32	33	SL	$2.485 * 10^3$	14.303	11.192	11.710

TABLE IV

EXPERIMENTAL AND CALCULATED DATA IN PIPE INCLINED 15°

Run	V_v	Δh_{max}	Δh_{min}	Δh_{ave}	Flow	G_v/Λ	ΔP_{max}	ΔP_{min}	ΔP_{ave}
Series No. 1. V_ℓ = 1.014						Series No. 1. $G_\ell\psi$ = 1.09 * 10^2			
1	1.981	37	25	30	→W-SL	7.455 * 10^2	2.984	-3.237	-0.645
2	3.135	34	29	31	W	1.242 * 10^2	1.429	-1.163	-0.126
3	4.807	34	30	32	W	1.905 * 10^3	1.429	-0.645	0.392
4	6.270	33	30.5	32.5	W	2.485 * 10^3	0.910	-0.385	0.651
5	9.405	34	31	33	→W-A-SL	3.727 * 10^3	1.429	-0.126	0.910
6	10.345	33.5	32	33	A-W-SL	4.100 * 10^3	1.169	0.392	0.910
7	13.376			35	A	5.301 * 10^3			1.947
8	16.720			36.5	A	6.627 * 10^3			2.726
9	18.601			39	→A-SL	2.373 * 10^3			4.021
Series No. 2. V_ℓ = 1.487						Series No. 2. $G_\ell\psi$ = 1.60 * 10^2			
10	3.135	36	29	32	W-SL	1.242 * 10^2	2.466	-1.163	0.392
11	4.702	38	29	33	→W-SL	1.863 * 10^2	3.503	-1.163	0.651
12	7.315	35	30	33	→W-SL	2.899 * 10^3	1.947	-0.645	0.910
13	10.450	38	30	34	→A-W-SL	4.142 * 10^3	3.503	-0.645	1.429
14	14.107			35	A	5.591 * 10^2			1.947
15	17.765			40	→A-SL	7.041 * 10^3			4.540
16	19.855			43	A	7.870 * 10^3			6.095
17	1.567			31.5	→W-ST	6.213 * 10^3			0.132
Series No. 3. V_ℓ = 3.110						Series No. 3. $G_\ell\psi$ = 3.34 * 10^2			
18	1.567	32	30	31.5	W	6.213 * 10^2	0.393	-0.645	0.132
19	5.225	34	30	32.5	W-SL	2.071 * 10^3	1.429	-0.645	0.651
20	7.315	35		32.8	→W-SL	2.899 * 10^3	1.947		0.806
21	9.927	44	32	38	SL	3.935 * 10^3	6.614	0.392	3.503
Series No. 4. V_ℓ = 0.901						Series No. 4. $G_\ell\psi$ = 9.7 * 10^1			
22	1.254	33	30	31	→W-ST	4.970 * 10^2	0.910	-0.645	-0.126
23	2.090	33.5	30	31.2	W	8.284 * 10^2	1.169	-0.645	-0.022
24	3.971	34		32	W-SL	1.574 * 10^3	1.429		0.392
25	6.061			32.8	W-SL	2.402 * 10^3			0.806
26	8.987	36	30	33.5	W-S	3.562 * 10^3	2.466	-0.645	1.169
27	12.122	37	31	34	→A-SL	4.804 * 10^3	2.984	-0.126	1.429
28	14.839			35	A	5.881 * 10^3			1.947
29	16.720			36	A	6.627 * 10^3			2.466
30	18.810			39	A	7.455 * 10^3			4.021
31	0.522			31.2	→ST-W	2.071 * 10^2			-0.022

TABLE IV (Continued)

Run	V_v	Δh_{max}	Δh_{min}	Δh_{ave}	Flow	G_v/Λ	ΔP_{max}	ΔP_{min}	ΔP_{ave}
Series No. 5. V_ℓ = 0.394						Series No. 5. $G_\ell\psi = 4.24 * 10^1$			
32	0.522	32.5	30	31.2	→ST-W	$2.071 * 10^2$	0.651	-0.645	-0.022
33	1.254	34.5	30	31.5	W	$4.970 * 10^2$	1.688	-0.645	0.132
34	3.135	34.5		32.1	W-SL	$1.242 * 10^3$	1.688		0.443
35	5.016	35		32.4	W-SL	$1.988 * 10^3$	1.947		0.599
36	7.524	34		32.5	W	$2.982 * 10^3$	1.429		0.651
37	10.450	33.5		32.5	W	$4.142 * 10^3$	1.169		0.703
38	14.630			34	A	$5.799 * 10^3$			1.429
39	16.720			35	A	$6.627 * 10^3$			1.947
40	19 855			37	A	$7.870 * 10^3$			2.984
Series No. 6. V_ℓ = 5.124						Series No. 6. $G_\ell\psi = 5.5 * 10^2$			
41	1.254	31.8	31	31.5	W	$4.970 * 10^2$	0.288	-0.126	0.132
42	3.135	33	31	32	W-SL	$1.242 * 10^3$	0.910	-0.126	0.392
43	5.225			33	W-SL	$2.071 * 10^3$			0.910
44	7.315	38		34	SL	$2.899 * 10^3$	3.503		1.429
45	8.360			38	SL-A	$3.313 * 10^3$			2.503
Series No. 7. V_ℓ = 0.129						Series No. 7. $G_\ell\psi = 1.39 * 10^1$			
46	1.045	31.5	31.3	31.4	ST	$4.142 * 10^2$	0.132	0.029	0.080
47	2.090	31.6	31.4	31.5	ST	$8.284 * 10^2$	0.184	0.080	0.132
48	3.135	31.65	31.45	31.6	ST	$1.242 * 10^3$	0.210	0.106	0.184
49	4.807	31.75	31.65	31.7	ST	$1.905 * 10^3$	0.262	0.210	0.236
50	6.061	31.8	31.65	31.75	→ST-W-SL	$2.402 * 10^3$	0.288	0.210	0.263
51	7.315	31.95	31.8	31.9	→ST-W-SL	$2.899 * 10^3$	0.366	0.288	0.340
52	9 405	32.1		32	ST-W-SL	$3.727 * 10^3$	0.443		0.392
53	10.241	32.3		32.2	W-SL	$4.059 * 10^3$	0.547		0.495
54	11.495	32.4	32	32.3	W-SL	$4.556 * 10^3$	0.599	0.392	0.547
55	14.212	32.9		32.7	W-SL-A	$5.633 * 10^3$	0.858		0.754
56	16.720	33.9		33.7	A	$6.627 * 10^3$	1.377		1.273
57	18.810			34 4	A	$7.455 * 10^3$			1.636
58	19.855			34.6	A	$7.870 * 10^3$			1.740
Series No. 8. V_ℓ = 0.564						Series No. 8. $G_\ell\psi = 6.06 * 10^1$			
59	7.315	32.5	31.5	32	→W-SL	$2.899 * 10^3$	0.651	0.132	0.392
60	1.045	32.5	31	31	SL-W	$4.142 * 10^2$	0.651	-0.126	-0.126
61	2.299			31	W-SL	$9.112 * 10^2$			-0.126
62	4.180			31.8	→W-SL	$1.656 * 10^3$			0.288
63	6.280	32.3		31.9	→W-SL	$2.485 * 10^3$	0.547		0.340
64	10.136	33.5	32	32.5	→W-A-SL	$4.017 * 10^3$	1.169	0.392	0.651
65	11.495			32.7	→A-SL	$4.556 * 10^3$			0.754
66	14.630	34.6	33.8	34	A	$5.799 * 10^3$	1.740	1.025	1.429

TABLE IV (Continued)

Run	V_v	Δh_{max}	Δh_{min}	Δh_{ave}	Flow	G_v/Λ	ΔP_{max}	ΔP_{min}	ΔP_{ave}
67	15.675			34.7	A	$6.213 * 10^3$			1.791
68	17.765			36.5	A	$7.041 * 10^3$			2.725
69	19.437			37.8	→A-SL	$7.704 * 10^3$			3.399
70	20.900			39.8	A	$8.284 * 10^3$			4.436
Series No. 9. $V_\ell = 1.825$						Series No. 9. $G_\ell\psi = 1.96 * 10^2$			
71	20.900	33	30	31.6	SL	$8.284 * 10^2$	0.910	-0.645	0.184
72	3.344	35	30	32	SL	$1.325 * 10^3$	1.947	-0.645	0.392
73	5.434	35.5		32.5	SL	$2.153 * 10^3$	2.206		0.651
74	7.524	36	31	33	→SL-A	$2.982 * 10^3$	7.460	-0.126	0.910
75	1.045			31.4	W-SL	$4.142 * 10^2$			0.080
76	10.136	35		33.5	→SL-A	$4.017 * 10^3$	1.947		1.169
77	11.704			34	→A-SL	$4.639 * 10^3$			1.429
78	15.257	39	36	37	A-SL	$6.047 * 10^3$	4.021	2.466	2.984
79	17.765			41	→A	$7.041 * 10^3$			5.058
Series No. 10. $V_\ell = 3.603$						Series No. 10. $G_\ell\psi = 3.87 * 10^2$			
80	0.836			31.5	B-W	$3.313 * 10^2$			0.132
81	2.09			31.6	B-SL	$8.284 * 10^2$			0.184
82	3.135	35	31	32	B-SL	$1.242 * 10^3$	1.947	-0.126	0.392
83	4.18			33.5	B-SL	$1.656 * 10^3$			1.169
84	5.225			34	→B-SL	$2.071 * 10^3$			1.947
85	6.479	37	32	35	→B-SL	$2.568 * 10^3$	2.98	0.392	2.466
86	8.360			36	SL	$3.313 * 10^3$			2.984
87	10.032			37	SL	$3.976 * 10^3$			0.158
88	0.522			31.55	W-B	$2.071 * 10^2$			0.080
Series No. 11. $V_\ell = 0.060$						Series No. 11. $G_\ell\psi = 6.45 * 10^0$			
89	2.508			31.4	ST	$9.941 * 10^2$			0.132
90	5.016			31.5	ST	$1.988 * 10^3$			0.184
91	7.942			31.6	ST	$3.148 * 10^3$			0.288
92	8.778			31.8	ST	$3.479 * 10^3$			0.392
93	9.823			32	ST	$3.893 * 10^3$			0.547
94	12.540			32.3	→W-SL-ST	$4.970 * 10^3$			1.117
95	17.556			33.4	→W-A-ST	$6.958 * 10^3$			1.377
96	18.810			33.9	→A-W	$7.455 * 10^3$			1.947
97	20.900			35	A-W	$8.284 * 10^3$			0.392
Series No. 12. $V_\ell = 0.744$						Series No. 12. $G_\ell\psi = 8.0 * 10^1$			
98	4.180	34	30	32	SL-W	$1.656 * 10^3$	1.429	-0.645	0.184
99	1.254			31.6	→W-SL	$4.970 * 10^2$			0.184
100	3.135	34	30	31.8	W-SL	$1.242 * 10^3$	1.429	-0.645	0.288
101	5.643	34	31	32.1	W-SL	$2.236 * 10^3$	1.429	-0.126	0.443

TABLE IV (Continued)

Run	V_v	Δh_{max}	Δh_{min}	Δh_{ave}	Flow	G_v/A	ΔP_{max}	ΔP_{min}	ΔP_{ave}
102	7.106	34	31	32.3	W-SL	$2.816 * 10^3$	1.429	-0.126	0.547
103	9.405	34.5	32	32.5	A-SL-W	$3\ 727 * 10^3$	1.688	0.392	0.651
104	12.540	34.5	32	33	→A-SL	$4.970 * 10^3$	1.688	0.392	0.910
105	15.675	36	34.5	35.5	A-SL	$6.213 * 10^3$	2.466	1.682	2.206
106	20.064	40	39	39.5	A-SL	$7.952 * 10^3$	4.540	4.021	4.280
Series No. 13. $V_\ell = 0.183$						Series No. 13. $G_\ell\Psi = 1.97 * 10^1$			
107	6.270			31.7	W-ST-SL	$2.485 * 10^3$			0.236
108	1.881			31.5	ST-W	$7.455 * 10^2$			0.132
109	4.389			31.6	W-ST	$1.739 * 10^3$			0.184
110	8.36			31.8	W	$3.313 * 10^3$			0.288
111	12.958			32.5	W-A	$5.136 * 10^3$			0.651
112	16.720			33.7	A	$6.627 * 10^3$			1.273
113	19.855			35.2	A	$7.870 * 10^3$			2.051
Series No. 14. $V_\ell = 2.122$						Series No. 14. $G_\ell\Psi = 2.28 * 10^2$			
114	1.881			32	B	$7.455 * 10^2$			0.392
115	1.254	32.5	31.5	31.8	B-SL	$4.970 * 10^2$	0.651	0.132	0.288
116	0.523	32		31.5	W-B-SL	$2.071 * 10^2$	0.392		0.132
117	2.090	35	30	32.5	B-SL	$8.284 * 10^2$	1.947	-0.645	0.651
118	3.135	35.5	31	33	B-SL	$1.242 * 10^3$	2.206	-0.126	0.910
119	4.389	36		33.5	B-SL	$1.739 * 10^3$	2.466		1.169
120	6.270	36	31	33.5	SL	$2.485 * 10^3$	2.466	-0.126	1.169
121	9.196	35.5		33.6	→A-SL	$3.645 * 10^3$	2.206		1.221
122	10.868	37	34	34.5	→A-SL	$4.307 * 10^3$	2.984	1.429	1.688
123	12,540	39	34.5	36	→A-SL	$4.970 * 10^3$	4.021	1.688	2.466
124	15.675	39	37	38	→A-SL	$6.213 * 10^3$	4.021	2.984	3.503
125	17.765	43		42	A	$7.041 * 10^3$	6.090		5.577
Series No. 15. $V_\ell = 4.354$						Series No. 15. $G_\ell\Psi = 4.68 * 10^2$			
126	0.627	31.6	31.4	31.5	B	$2.485 * 10^2$	0.184	0.080	0.132
127	1.463		31.5	32	B	$5.799 * 10^2$		0.132	0.392
128	2.403	33.5	32	32.5	B-SL	$9.526 * 10^2$	1.169	0.392	0.651
129	3.657	34.5	32.5	33	B-SL	$1.449 * 10^3$	1.688	0.651	0.910
130	5.225	36	32.8	33.5	B-SL	$2.071 * 10^3$	2.466	0.806	1.169
131	7.315	36	33	34	B-SL	$2.899 * 10^3$	2.466	0.910	1.429
132	8.569	39	34	36	→A-SL	$3.396 * 10^3$	4.021	1.429	2.466
133	10.450	40		38	→A-SL	$4.142 * 10^3$	4.540		3.503

VITA

Domingo L. Moreno Beltrán

Candidate for the Degree of

Master of Science

Thesis: TWO-PHASE FLOW IN AN INCLINED PIPE

Major Field: Chemical Engineering

Biographical:

Personal Data: Born in Valencia, Spain, February 25, 1946, the son of Domingo Moreno Garcia and Josefa Beltran Martinez

Education: Attended Luis Vives High School , Valencia, Spain, in June, 1963; graduated from Superior Technical School of Industrial Engineering with the Diploma of Ingeniero Industrial, in July, 1970; completed requirements for the Master of Science degree at Oklahoma State University in July, 1972.

Professional Experience: Employed by Altos Hornos de Vizcaya, Sagunto (Valencia), Spain, during the summer of 1966; employed by IJsselcentrale-Zwolle, Netherlands, during the summer of 1967; employed by Metra Seis, Madrid, Spain, during the spring of 1969; employed as teaching assistant Superior Technical School of Industrial Engineering, Madrid, Spain, during the fall of 1969.